INTERNATIONAL JOURNAL FOR NUMERICAL METHODS IN ENGINEERING
Int. J. Numer. Meth. Engng 2003; **56**:2135–2161 (DOI: 10.1002/nme.657)

A study on finite elements for capturing strong discontinuities

J. Oliver*,†, A. E. Huespe‡ and E. Samaniego

E.T.S. Enginyers de Camins, Canals i Ports, Technical University of Catalonia, Campus Nord UPC, Mòdul C1, Gran Capitán s/n, 08034 Barcelona, Spain

SUMMARY

The work focuses on the presently existing families of finite elements with embedded discontinuities and explores the possibilities of obtaining symmetric statically consistent finite elements that alleviate the stress-locking problem. For this purpose, mixed (reduced integration) and assumed enhanced strain techniques are applied to the basic symmetric four-noded element. Numerical simulations show the effectiveness of the proposed measures. Copyright © 2003 John Wiley & Sons, Ltd.

KEY WORDS: finite elements; embedded discontinuities; strong discontinuities; mixed elements; assumed enhanced strains

1. MOTIVATION

In recent years, the so called *finite elements with embedded discontinuities* have been the subject of increasing study and development [1–12]. Its rising popularity comes from the fact that, by using these elements, a displacement discontinuity model can be introduced in the bulk of the element (and therefore regardless of the orientation of its sides) in combination with appropriate propagation mechanisms. Moreover, it has been shown [6] that in strain localization scenarios, some of those elements completely overcome the well-known problem of the spurious mesh size and mesh orientation dependence of the results [13].

Although there are quite different families of such elements, apparently, not all of them behave in the same way. A fairly comprehensive study of the different families can be found in Reference [14]. They can be classified into three different groups:

(i) *Symmetric statically consistent elements*. Traction continuity across the discontinuity interface is introduced in a fully consistent variational environment that results in a

*Correspondence to: J. Oliver, E.T.S. Enginyers de Camins, Canals i Ports, Technical University of Catalonia, Campus Nord UPC, Mòdul C1, Gran Capitán s/n, 08034 Barcelona, Spain.
†E-mail: oliver@cimne.upc.es
‡CIMEC/CONICET-UNL, Argentina. E-mail: ahuespe@intec.unl.edu.ar

Received 11 September 2001
Revised 7 March 2002
Accepted 10 June 2002

symmetric formulation. However, the way of introducing the discontinuous kinematics does not guarantee free rigid body relative motions of the two portions of the element split up into by the discontinuity.[§] A description of such formulation can be found in Reference [8].

(ii) *Symmetric kinematically consistent elements*. The kinematics is introduced in a way that does not restrict the rigid body relative motions of the two portions of the element. However, traction continuity across the discontinuous interface is not guaranteed at elemental level. A typical triangular element based on this formulation can be found in Reference [5].

(iii) *Non-symmetrical statically and kinematically consistent elements.* Both the rigid body relative motions and the traction continuity are introduced at the elemental level, but the second is introduced in a strong form that makes the resulting formulation non-symmetrical. Typically, these are the formulations used in References [6] and [7].

From the authors' experiences the last family of elements (iii) is the one that provides more robust and reliable results and they have used it successfully for numerical simulations in many different settings [15–21]. Family (ii) exhibits also a robust behaviour although a much slower convergence with mesh refinement, whereas family (i), as will be shown below, exhibits in many cases the well-known stress locking phenomenon.

However, although the fact that formulation (iii) is not symmetric is neither a fundamental drawback nor a source of unbearable computational costs, the variational consistency of formulation (i) agrees with the *traditional* finite element technology in Computational Solid Mechanics and confers additional appeal upon it. More important, the symmetric elements of family (i) can be theoretically derived *without the necessity of the tracking algorithm concept* which appears to be a fundamental issue on the other two families and sets practical difficulties to generalize its use for capturing multiple cracking and branching phenomena.

This is why this paper is devoted to exploring and developing several new types of finite elements with embedded discontinuities belonging to this family. However, and since the aforementioned stress locking phenomena makes the basic formulation unsuitable, specific treatments are explored to face that problem. *Mixed and assumed enhanced strain techniques* are envisaged as appropriated remedies, so that they are introduced in the basic element and their effects on the stress locking are analysed.

1.1. The boundary value problem

Let us consider the body Ω of Figure 1(a), undergoing a (rate of) displacement discontinuity $[\![\dot{\mathbf{u}}]\!](\mathbf{x},t)$ across the material (fixed) surface $\mathscr{S}$ that splits the body into Ω^+ (pointed by the unit normal $\mathbf{n}$ to $\mathscr{S}$) and Ω^- such that $\Omega^+ \cup \Omega^- = \Omega \backslash \mathscr{S}$.[¶] The resulting velocity, $\dot{\mathbf{u}}(\mathbf{x},t)$, and

[§] As will be shown in subsequent sections this can result in *stress locking* behaviour.

[¶] Notation $A \backslash B$ stands for the result of subtraction of domain B from domain A.

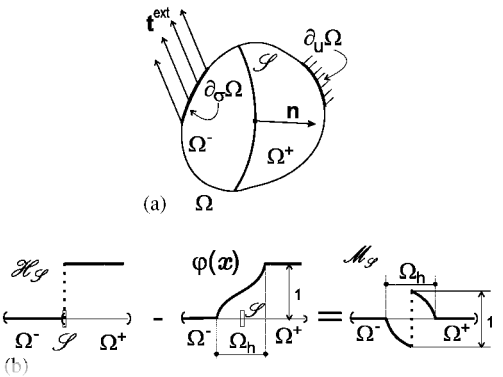

Figure 1. (a) Continuum body with a displacement discontinuity; and (b) construction of the $\mathscr{M}_{\mathscr{S}}(\mathbf{x})$ function.

strain rate, $\dot{\boldsymbol{\varepsilon}}(\mathbf{x},t)$, fields[‖] can be expressed as in [20]:

$$\begin{aligned}
&\dot{\mathbf{u}}(\mathbf{x},t) = \bar{\dot{\mathbf{u}}}(\mathbf{x},t) + \mathscr{M}_{\mathscr{S}}[\![\dot{\mathbf{u}}]\!](\mathbf{x},t)\\
&[\![\dot{\mathbf{u}}]\!] = \dot{\mathbf{u}}|_{\mathbf{x}\in\partial\Omega^+\cap\mathscr{S}} - \dot{\mathbf{u}}|_{\mathbf{x}\in\partial\Omega^-\cap\mathscr{S}}; \qquad \bar{\dot{\mathbf{u}}} = \dot{\mathbf{u}}^* \quad \text{in } \partial_u\Omega \qquad (1)\\
&\dot{\boldsymbol{\varepsilon}}(\mathbf{x},t) = \nabla^S\dot{\mathbf{u}}(\mathbf{x},t) = \underbrace{\bar{\dot{\boldsymbol{\varepsilon}}}}_{\substack{\text{regular}\\(\text{bounded})}} + \underbrace{\delta_{\mathscr{S}}([\![\dot{\mathbf{u}}]\!]\otimes\mathbf{n})^S}_{\substack{\text{singular}\\(\text{unbounded})}}
\end{aligned}$$

$$\mathscr{M}_{\mathscr{S}}(\mathbf{x}) = \mathscr{H}_{\mathscr{S}}(\mathbf{x}) - \varphi(\mathbf{x}); \quad \varphi(\mathbf{x})\in H^1(\Omega) = \begin{cases} 1 & \forall\mathbf{x}\in\Omega^+\backslash\Omega_h\\ 0 & \forall\mathbf{x}\in\Omega^-\backslash\Omega_h \end{cases} \qquad (2)$$

where $[\![\dot{\mathbf{u}}]\!]$ stands for the velocity jump, $\partial_u\Omega$ is the part of the external boundary of Ω (with outward normal $\mathbf{v}$) where displacements are prescribed to $\mathbf{u}^*(\mathbf{x},t)$, $\mathscr{H}_{\mathscr{S}}$ is the Heaviside's jump function placed on $\mathscr{S}$ ($\mathscr{H}_{\mathscr{S}}(\mathbf{x})=1\ \forall\mathbf{x}\in\Omega^+$ and $\mathscr{H}_{\mathscr{S}}(\mathbf{x})=0\ \forall\mathbf{x}\in\Omega^-$), $\mathscr{M}_{\mathscr{S}}$ is a unit jump function, whose support is a certain domain Ω_h containing $\mathscr{S}$ (see Figure 1(b)) and constructed as it is indicated in Equation (2), and $\delta_{\mathscr{S}}$ is the Dirac's delta function placed on $\mathscr{S}$ that arises from the derivation of the discontinuous function $\mathscr{M}_{\mathscr{S}}(\mathbf{x})$.

The corresponding quasistatic boundary value problem (BVP) can be described, in rate form, as the following three field, $\mathbf{u}$–$\boldsymbol{\varepsilon}$–$\boldsymbol{\sigma}$, problem:

$$\textit{Find}: \begin{cases} \dot{\mathbf{u}}(\mathbf{x},t)\\ \dot{\boldsymbol{\varepsilon}}(\mathbf{x},t)\\ \dot{\boldsymbol{\sigma}}(\mathbf{x},t) \end{cases} \quad \text{satisfying:}$$

[‖]The mathematical expressions of the resulting *continuum format* kinematics is referred to as *strong discontinuity kinematics* [20].

$$\nabla \cdot \dot{\boldsymbol{\sigma}} + \dot{\mathbf{b}} = \mathbf{0} \quad \text{in } \Omega \backslash \mathscr{S} \quad \text{(internal equilibrium)} \tag{3a}$$

$$\dot{\boldsymbol{\varepsilon}} - \nabla^{\mathrm{S}} \dot{\mathbf{u}} = \mathbf{0} \quad \text{in } \Omega \quad \text{(kinematical compatibility)} \tag{3b}$$

$$\dot{\boldsymbol{\sigma}} - \dot{\boldsymbol{\Sigma}}(\boldsymbol{\varepsilon}) = \mathbf{0} \quad \text{in } \Omega \quad \text{(constitutive compatibility)} \tag{3c}$$

$$\dot{\boldsymbol{\sigma}} \cdot \boldsymbol{\nu} = \dot{\mathbf{t}}^{\mathrm{ext}} \quad \text{on } \partial_\sigma \Omega \quad \text{(external equilibrium)} \tag{3d}$$

$$\underbrace{\dot{\boldsymbol{\sigma}}_{\Omega^+} \cdot \mathbf{n} - \dot{\boldsymbol{\sigma}}_{\Omega^-} \cdot \mathbf{n}}_{\stackrel{\text{def}}{=}[[\dot{\boldsymbol{\sigma}}]]_{\Omega \backslash \mathscr{S}} \cdot \mathbf{n}} = \mathbf{0} \quad \text{on } \mathscr{S} \quad \text{(outer traction continuity)} \tag{3e}$$

$$\underbrace{\dot{\boldsymbol{\sigma}}_{\Omega^+} \cdot \mathbf{n} - \dot{\boldsymbol{\sigma}}_{\mathscr{S}} \cdot \mathbf{n}}_{\stackrel{\text{def}}{=}[[\dot{\boldsymbol{\sigma}}]]_{\mathscr{S}} \cdot \mathbf{n}} = \mathbf{0} \quad \text{on } \mathscr{S} \quad \text{(inner traction continuity)} \tag{3f}$$

where $\boldsymbol{\sigma}(\mathbf{x}, t)$ stands for the stresses, $\mathbf{b}(\mathbf{x}, t)$ are the body forces density, $\boldsymbol{\Sigma}(\boldsymbol{\varepsilon})$ stands for the constitutive function returning the stresses in terms of the strains $\boldsymbol{\varepsilon}$ and $\partial_\sigma \Omega$ is the part of the boundary of Ω where tractions $\mathbf{t}^{\mathrm{ext}}$ are prescribed. Equations (3e) and (3f) state the continuity of the traction vector $\mathscr{T} = \boldsymbol{\sigma} \cdot \mathbf{n}$ through the discontinuity interface $\mathscr{S}$. After explicit imposition of condition (3c) BVP (3) can be rewritten as a two field, $\mathbf{u}$–$\boldsymbol{\varepsilon}$, problem:

$$\textit{Find:} \quad \begin{cases} \dot{\mathbf{u}}(\mathbf{x}, t) \\ \dot{\boldsymbol{\varepsilon}}(\mathbf{x}, t) \end{cases} \quad \text{satisfying:}$$

$$\nabla \cdot \dot{\boldsymbol{\Sigma}} - \dot{\mathbf{b}} = \mathbf{0} \quad \text{in } \Omega \backslash \mathscr{S} \quad \text{(internal equilibrium)} \tag{4a}$$

$$\dot{\boldsymbol{\varepsilon}} - \nabla^{\mathrm{S}} \dot{\mathbf{u}} = \mathbf{0} \quad \text{in } \Omega \quad \text{(kinematical compatibility)} \tag{4b}$$

$$\dot{\boldsymbol{\Sigma}} \cdot \boldsymbol{\nu} = \dot{\mathbf{t}}^{\mathrm{ext}} \quad \text{on } \partial_\sigma \Omega \quad \text{(external equilibrium)} \tag{4c}$$

$$\underbrace{\dot{\boldsymbol{\Sigma}}_{\Omega^+} \cdot \mathbf{n} - \dot{\boldsymbol{\Sigma}}_{\Omega^-} \cdot \mathbf{n}}_{\stackrel{\text{def}}{=}[[\dot{\boldsymbol{\Sigma}}]]_{\Omega \backslash \mathscr{S}} \cdot \mathbf{n}} = \mathbf{0} \quad \text{on } \mathscr{S} \quad \text{(outer traction continuity)} \tag{4d}$$

$$\underbrace{\dot{\boldsymbol{\Sigma}}_{\Omega^+} \cdot \mathbf{n} - \dot{\boldsymbol{\Sigma}}_{\mathscr{S}} \cdot \mathbf{n}}_{\stackrel{\text{def}}{=}[[\dot{\boldsymbol{\Sigma}}]]_{\mathscr{S}} \cdot \mathbf{n}} = \mathbf{0} \quad \text{on } \mathscr{S} \quad \text{(inner traction continuity)} \tag{4e}$$

2. NON-SYMMETRIC (PETROV–GALERKIN) APPROACH

A weak form of the BVP (4) can be devised as follows. In view of the velocity field (1) let us consider the functional spaces of the velocities, $\mathscr{V}_{\mathbf{u}}$, and virtual (kinematically admissible) velocities, $\bar{\mathscr{V}}_{\mathbf{u}}^0$:

$$\begin{aligned} \mathscr{V}_{\mathbf{u}} &\stackrel{\text{def}}{\equiv} \{\boldsymbol{\eta}(\mathbf{x}) = \bar{\boldsymbol{\eta}} + \mathscr{M}_{\mathscr{S}}\, \boldsymbol{\alpha};\ \bar{\boldsymbol{\eta}} \in [\mathsf{H}^1(\Omega)]^{n_{\mathrm{dim}}};\ \boldsymbol{\alpha} \in \mathsf{L}_2(\mathscr{S})\} \\ \bar{\mathscr{V}}_{\mathbf{u}}^0 &\stackrel{\text{def}}{\equiv} \{\bar{\boldsymbol{\eta}}^0(\mathbf{x}) \in [\mathsf{H}^1(\Omega)]^{n_{\mathrm{dim}}};\ \bar{\boldsymbol{\eta}}^0|_{\partial_u \Omega} = \mathbf{0}\} \end{aligned} \tag{5}$$

where n_{dim} stands for the number of dimensions of the problem, $\mathsf{H}^1(\Omega)$ is the functional space of functions defined in Ω with square integrable first derivatives and $\mathsf{L}_2(\mathscr{S})$ the functional space of square integrable functions defined in $\mathscr{S}$.**

Remark 1
Notice that spaces $\mathscr{V}_{\bar{\mathbf{u}}}$ and $\mathscr{V}_{\mathbf{u}}^0$ differ not only for the homogeneous boundary condition imposed to the elements of $\mathscr{V}_{\mathbf{u}}^0$, but also for the intrinsic nature of their elements $\boldsymbol{\eta}(\mathbf{x}) = \bar{\boldsymbol{\eta}} + \mathscr{M}_{\mathscr{S}}\boldsymbol{\alpha}$ and $\bar{\boldsymbol{\eta}}^0(\mathbf{x})$, respectively. This fact entails the non-symmetric character of the resulting formulation.

In view of the preceding notation the weak form of the problem can be written:

Problem 1 (*Continuous non-symmetric problem*)

Find

$$\begin{aligned} \dot{\mathbf{u}} &= \dot{\bar{\mathbf{u}}} + \mathscr{M}_{\mathscr{S}}[\![\dot{\mathbf{u}}]\!]; \quad \dot{\mathbf{u}} \in \mathscr{V}_{\bar{\mathbf{u}}} \\ \dot{\boldsymbol{\varepsilon}} &= \nabla^{\mathrm{S}}\dot{\mathbf{u}} = \dot{\bar{\boldsymbol{\varepsilon}}} + \delta_s([\![\dot{\mathbf{u}}]\!] \otimes \mathbf{n})^{\mathrm{S}} \end{aligned} \tag{6}$$

Such that

$$\delta\Pi_u(\dot{\boldsymbol{\Sigma}}; \eta) = \int_{\Omega\setminus\mathscr{S}} \dot{\boldsymbol{\Sigma}}(\nabla^{\mathrm{S}}\dot{\mathbf{u}}) : \nabla^{\mathrm{S}}\boldsymbol{\eta}\, \mathrm{d}\Omega - \underbrace{\int_{\Omega\setminus\mathscr{S}} \dot{\mathbf{b}} \cdot \boldsymbol{\eta}\, \mathrm{d}\Omega + \int_{\partial_\sigma\Omega} \dot{\mathbf{t}} \cdot \boldsymbol{\eta}\, \mathrm{d}\Gamma}_{G_{\text{ext}}} = 0 \quad \forall \boldsymbol{\eta} \in \mathscr{V}_{\mathbf{u}}^0 \tag{7}$$

Some standard calculations show that the strong form of Problem 1 is

$$\delta\Pi_u(\mathbf{u}; \boldsymbol{\eta}) = 0 \;\Rightarrow\; \begin{cases} \nabla \cdot \dot{\boldsymbol{\Sigma}} + \dot{\mathbf{b}} = \mathbf{0} & \text{in } \Omega\setminus\mathscr{S} \\ \dot{\boldsymbol{\Sigma}} \cdot \boldsymbol{\nu} = \dot{\mathbf{t}}^{\text{ext}} & \text{on } \partial_\sigma\Omega \\ [\![\dot{\boldsymbol{\Sigma}}]\!]_{\mathscr{S}} \cdot \mathbf{n} = 0 & \text{on } \mathscr{S} \end{cases} \tag{8}$$

and, therefore, only condition (4e) remains to be fulfilled in the BVP defined by Equations (4). This condition is going to be imposed via a different procedure in the finite element formulation, essentially in strong form. In summary the BVP (4) is approached as:

$$\begin{aligned} \delta\Pi_u(\dot{\boldsymbol{\Sigma}}(\dot{\bar{\mathbf{u}}}, [\![\dot{\mathbf{u}}]\!]); \boldsymbol{\eta}) = 0 \quad \forall \boldsymbol{\eta} \in \mathscr{V}_{\mathbf{u}}^0 \quad &\text{(variational/weak form)} \\ [[\dot{\boldsymbol{\Sigma}}_{\mathscr{S}}]] \cdot \mathbf{n} = \mathbf{0} \quad \text{on } \mathscr{S} \quad &\text{(strong form)} \end{aligned} \tag{9}$$

2.1. Finite element discretization (standard non-symmetric element: U4n)

Let us consider the material domain Ω discretized in a four-noded†† finite element mesh with n_{elem} elements and n_{node} nodes crossed by the discontinuity interface $\mathscr{S}$ (see Figure 2(a)). Let us assume that an available *discontinuity tracking algorithm* [6] determines the subset $\mathscr{J}$ of the $n_{\mathscr{J}}$ elements that are crossed by $\mathscr{S}$ at the considered time t:

$$\mathscr{J} := \{e \,|\, \Omega_e \cap \mathscr{S} \neq \emptyset\} = \{e_i, \ldots, e_m, \ldots e_p, \ldots\} \tag{10}$$

**Roughly $\mathsf{H}^1(\cdot)$ contains continuous function defined in $(\cdot)$ with discontinuous first derivatives and $\mathsf{L}_2(\cdot)$ contains piecewise discontinuous bounded functions defined in $(\cdot)$.
††For the sake of simplicity, from now on only two-dimensional problems will be considered.

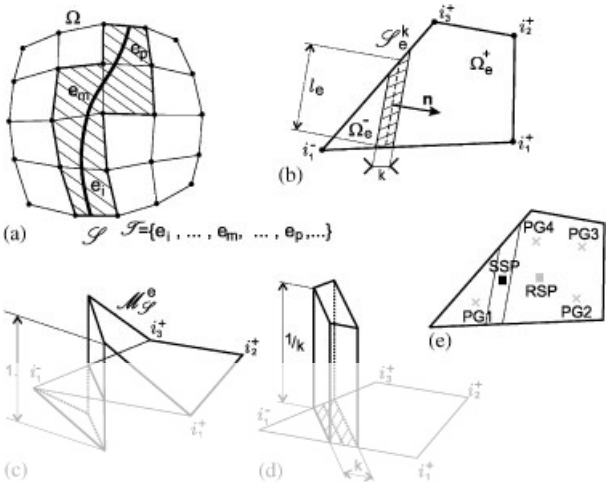

Figure 2. 2D discretization by using quadrilateral elements: (a) set $\mathscr{J}$ of elements intersected by the discontinuity; (b) elemental discontinuity $\mathscr{S}_e$; (c) function $\mathscr{M}_{\mathscr{J}}$; (d) regularized Delta's function; and (e) sampling points involved in the numerical integration.

For every element of $\mathscr{J}$, the tracking algorithm[‡‡] also provides the position of the elemental discontinuity interface $\mathscr{S}_e$ (see Figure 2(b) of length l_e which defines the domains Ω_e^+ and Ω_e^- and the nodes $i^+ \in \{i_1^+, \ldots, i_{n_e^+}^+\}$ and $i^- \in \{i_1^-, \ldots, i_{n_e^-}^-\}$). Now, the following interpolation of the velocity field $\dot{\mathbf{u}}^{(e)}$ inside a given element e is considered [6]:

$$\dot{\mathbf{u}}^{(e)}(\mathbf{x},t) = \underbrace{\sum_{i=1}^{i=4} N_i^{(e)}(\mathbf{x})\dot{\mathbf{d}}_i(t)}_{\dot{\bar{\mathbf{u}}}^{(e)}} + \underbrace{\mathscr{M}_{\mathscr{J}}^{(e)}(\mathbf{x})\,[[\dot{\mathbf{u}}]]_e(t)}_{\dot{\tilde{\mathbf{u}}}^{(e)}} \tag{11}$$

where $\dot{\bar{\mathbf{u}}}^{(e)}$ is the standard $\mathscr{C}^0$ velocity field, interpolated by the shape functions $\{N_1^{(e)}, N_2^{(e)}, N_3^{(e)}, N_4^{(e)}\}$ of the linear isoparametric quadrilateral element [22], in terms of the nodal velocities $\mathbf{d}_i(t)$ at node i. The term $\dot{\tilde{\mathbf{u}}}^{(e)}$, in Equation (11), captures the singular (discontinuous) part of the velocity field (1) in terms of the *elemental velocity jump* $[[\dot{\mathbf{u}}]]_e$ and $\mathscr{M}_{\mathscr{J}}^e(\mathbf{x})$ is the discrete counterpart of the unit jump function in Equation (2) defined as follows:

$$\mathscr{M}_{\mathscr{J}}^{(e)}(\mathbf{x}) = \begin{cases} 0 & \forall e \notin \mathscr{J} \\ \mathscr{H}_{\mathscr{J}}^{(e)}(\mathbf{x}) - \varphi^{(e)} \\ \left(\varphi^{(e)} = \sum_{i^+=1}^{n_e^+} N_{i^+}\right) & \forall e \in \mathscr{J} \end{cases} \tag{12}$$

where $\mathscr{H}_{\mathscr{J}}^{(e)}$ is the step function. Figure 2(c) shows the $\mathscr{M}_{\mathscr{J}}^{(e)}$ function and emphasizes its elemental support.

[‡‡]This tracking algorithm is a crucial ingredient of the non-symmetric formulations and constitute one of their most typical servitudes.

From Equations (11) and (12), the discrete (rate of) strain field reads

$$\dot{\boldsymbol{\varepsilon}}^{(e)} = \nabla^{\mathrm{S}}\dot{\mathbf{u}}^{(e)} = \sum_{i=1}^{i=4}(\nabla N_i^{(e)} \otimes \dot{\mathbf{d}}_i)^{\mathrm{S}} - (\nabla\varphi^{(e)} \otimes [[\dot{\mathbf{u}}]]_e)^{\mathrm{S}} + \delta_{\mathscr{S}}([\![\dot{\mathbf{u}}]\!]_e \otimes \mathbf{n})^{\mathrm{S}} \tag{13}$$

Notice that Equation (13) matches the strong discontinuity kinematics (1). In order to overcome the numerical difficulties of treating with the Dirac's delta function $\delta_{\mathscr{S}}$ it is replaced by a regularized[§§] function $\delta^e_{\mathscr{S}}$ defined within the element e as

$$\delta^{(e)}_{\mathscr{S}} = \mu^{(e)}_{\mathscr{S}} \frac{1}{k} \tag{14}$$

where $\mu^{(e)}_{\mathscr{S}}$ is a collocation function whose support is the domain $\mathscr{S}^k_e$ in Figure 2(d) defined in terms of the regularization parameter k:

$$\begin{aligned} \mu^{(e)}_{\mathscr{S}}(\mathbf{x}) &= 1 \quad \forall \mathbf{x} \in \mathscr{S}^k_e \\ \mu^{(e)}_{\mathscr{S}}(\mathbf{x}) &= 0 \quad \forall \mathbf{x} \notin \mathscr{S}^k_e \end{aligned} \tag{15}$$

By considering Equations (14) and (15) the regularized form of the strain rate field reads

$$\dot{\boldsymbol{\varepsilon}}^{(e)} = \nabla^{\mathrm{S}}\dot{\mathbf{u}}^{(e)} = \sum_{i=1}^{i=4}(\nabla N_i^{(e)} \otimes \dot{\mathbf{d}}_i)^{\mathrm{S}} - (\nabla\varphi^{(e)} \otimes [[\dot{\mathbf{u}}]]_e)^{\mathrm{S}} + \mu^{(e)}_{\mathscr{S}} \frac{1}{k}(\mathbf{n} \otimes [[\dot{\mathbf{u}}]]_e)^{\mathrm{S}} \tag{16}$$

In order to integrate the discontinuous terms emerging from the second term of the right-hand side of Equation (16), in addition to the standard sampling points of the linear quadrilateral (PG1 to PG4 in Figure 2(e)), the element is equipped with another integration point (SSP in Figure 2(d)) placed at the centre of the element and whose associated area is (see Figure 2(d))

$$\text{measure}(\mathscr{S}^k_e) = k l_e \tag{17}$$

The regularization parameter k has an arbitrary small value (as small as permitted by the machine precision).

In this context the inner traction continuity condition in Equations (4e) and (9) can be imposed on an element basis in terms of averages:

$$\dot{\boldsymbol{\Sigma}}_{\Omega^+} \cdot \mathbf{n} = (\dot{\boldsymbol{\Sigma}}_{\Omega^-} \cdot \mathbf{n}) = \dot{\boldsymbol{\Sigma}}_{\mathscr{S}} \cdot \mathbf{n} \rightarrow \underbrace{\frac{1}{\Omega_e}\int_{\Omega_e} \dot{\boldsymbol{\Sigma}} \cdot \mathbf{n}\, \mathrm{d}\Omega}_{\text{mean value on } \Omega\backslash\mathscr{S}} = \underbrace{\frac{1}{l_e}\int_{\mathscr{S}_e} \dot{\boldsymbol{\Sigma}} \cdot \mathbf{n}\, \mathrm{d}\Omega}_{\text{mean value on } \mathscr{S}} \tag{18}$$

$$\Rightarrow \int_{\Omega_e} \left(\mu^{(e)}_{\mathscr{S}} \frac{1}{k} - \frac{l_e}{\Omega_e}\right) \mathbf{n} \cdot \dot{\boldsymbol{\Sigma}}\, \mathrm{d}\Omega = \mathbf{0} \quad \forall e \in \mathscr{J} \tag{19}$$

[§§] This procedure and the resulting formulation have been sometimes termed in the literature the *regularized strong discontinuity approach.*

In view of the previous finite element discretization, and by resorting to the classical finite element procedures, the discrete counterpart of the BVP in Equations (9) can be written as follows:

Problem 2 (*Discrete non-symmetric problem*)

Given

$$\mathscr{V}_{\mathbf{u}}^{\mathrm{h}} \overset{\text{def}}{\equiv} \left\{ \boldsymbol{\eta}^{\mathrm{h}}(\mathbf{x}) = \sum_{i=1}^{i=n_{\text{node}}} N_i(\mathbf{x})\,\boldsymbol{\eta}_i + \sum_{e\in\mathscr{J}} \mathscr{M}_{\mathscr{S}}^{(e)}(\mathbf{x})\alpha_e \right\}$$
$$\bar{\mathscr{V}}_{\mathbf{u}}^{\mathrm{h}^0} \overset{\text{def}}{\equiv} \left\{ \boldsymbol{\eta}^{\mathrm{h}^0}(\mathbf{x}) = \sum_{i=1}^{i=n_{\text{node}}} N_i(\mathbf{x})\,\boldsymbol{\eta}_i^0;\ \ \boldsymbol{\eta}_i^0|_{\partial_u\Omega} = \mathbf{0} \right\} \tag{20}$$

Find

$$\dot{\mathbf{u}}^{\mathrm{h}} = \sum_{i=1}^{i=n_{\text{node}}} N_i\dot{\mathbf{d}}_i + \sum_{e\in\mathscr{J}} \mathscr{M}_{\mathscr{S}}^{(e)}(\mathbf{x})[[\dot{\mathbf{u}}]]_e;\quad \dot{\mathbf{u}}^{\mathrm{h}} \in \mathscr{V}_{\mathbf{u}}^{\mathrm{h}}$$
$$\dot{\boldsymbol{\varepsilon}}^{\mathrm{h}} = \nabla^{\mathrm{S}}\dot{\mathbf{u}}^{\mathrm{h}} = \sum_{i=1}^{i=n_{\text{node}}} (\nabla N_i \otimes \dot{\mathbf{d}}_i)^{\mathrm{S}} + \sum_{e\in\mathscr{J}} \left(\left[\mu_{\mathscr{S}}^{(e)} \frac{1}{k}\mathbf{n} - \nabla\varphi^{(e)} \right] \otimes [[\dot{\mathbf{u}}]]_e \right)^{\mathrm{S}} \tag{21}$$

Such that

$$\delta\Pi_u(\dot{\boldsymbol{\Sigma}}; \boldsymbol{\eta}^{\mathrm{h}}) = \sum_{e=1}^{e=n_{\text{elem}}} \int_{\Omega_e} \nabla^{\mathrm{S}}\boldsymbol{\eta}^{\mathrm{h}} : \dot{\boldsymbol{\Sigma}}(\varepsilon^{\mathrm{h}})\,\mathrm{d}\Omega - G_{\text{ext}} = 0 \quad \forall \boldsymbol{\eta}^{\mathrm{h}} \in \bar{\mathscr{V}}_{\mathbf{u}}^{\mathrm{h}^0}$$
$$[[\dot{\boldsymbol{\Sigma}}]]_{\mathscr{S}} \cdot \mathbf{n} = \mathbf{0} \rightarrow \int_{\Omega_e} \left(\mu_{\mathscr{S}}^{(e)} \frac{1}{k} - \frac{l_e}{\Omega_e} \right) \mathbf{n} \cdot \dot{\boldsymbol{\Sigma}}\,\mathrm{d}\Omega = \mathbf{0} \quad \forall e \in \mathscr{J} \tag{22}$$

The structure of Equations (22) corresponds to a typical Petrov–Galerkin residual weighting procedure [22] of the original BVP (4).

2.1.1. 2D implementation. For the two-dimensional case, in a cartesian coordinate system (x, y), using the vector format for the strains $\{\varepsilon\} = [\varepsilon_{xx}, \varepsilon_{yy}, 2\varepsilon_{xy}]^{\mathrm{T}}$ and the stresses $\{\sigma\} = [\sigma_{xx}, \sigma_{yy}, \sigma_{xy}]^{\mathrm{T}}$ (where $(\cdot)^{\mathrm{T}}$ stands for the transpose of $(\cdot)$), considering the four-noded quadrilateral as underlaying element and using the standard finite element *B-format* [22] Equations (22) yield

$$\left.\begin{aligned} \delta\Pi_u(\dot{\boldsymbol{\Sigma}}; \boldsymbol{\eta}^{\mathrm{h}}) = 0 \\ [[\dot{\boldsymbol{\Sigma}}]]_{\mathscr{S}} \cdot \mathbf{n} = \mathbf{0} \end{aligned}\right\} \rightarrow \bigcup_{e=1}^{e=n_{\text{elem}}} \left[\int_{\Omega_e} \mathbf{B}^{(e)^{\mathrm{T}}} \cdot \dot{\boldsymbol{\Sigma}}(\{\varepsilon\}^{(e)})\,\mathrm{d}\Omega - \dot{\mathbf{F}}^{\text{ext}(e)} \right] = \mathbf{0} \tag{23}$$

where $\dot{\mathbf{F}}^{\text{ext}(e)}$ stands for the classical elemental external forces vector and

$$\{\dot{\boldsymbol{\varepsilon}}\}^{(e)} = \mathbf{B}^{*(e)} \cdot \dot{\mathbf{d}}^{(e)}$$
$$\dot{\mathbf{d}}^{(e)} = [\dot{\mathbf{d}}_1,\ \dot{\mathbf{d}}_2,\ \dot{\mathbf{d}}_3,\ \dot{\mathbf{d}}_4,\ [[\dot{\mathbf{u}}]]_e]^{\mathrm{T}} \tag{24}$$

$$\mathbf{B}^{(e)} = [\mathbf{B}_1^{(e)},\ \mathbf{B}_3^{(e)},\ \mathbf{B}_4^{(e)},\ \mathbf{G}^{(e)}]$$

$$\mathbf{B}^{*(e)} = [\mathbf{B}_1^{(e)},\ \mathbf{B}_2^{(e)},\ \mathbf{B}_3^{(e)},\ \mathbf{B}_4^{(e)},\ \mathbf{G}^{*(e)}]$$

$$\mathbf{B}_i^{(e)} = \begin{bmatrix} \partial_x N_i^{(e)} & 0 \\ 0 & \partial_y N_i^{(e)} \\ \partial_y N_i^{(e)} & \partial_x N_i^{(e)} \end{bmatrix}$$

$$\mathbf{G}^{(e)} = \left(\mu_{\mathscr{S}}^{(e)} \frac{1}{k} - \frac{l_e}{\Omega_e} \right) \begin{bmatrix} n_x & 0 \\ 0 & n_y \\ n_y & n_x \end{bmatrix} \tag{25}$$

$$\mathbf{G}^{*(e)} = \mu_{\mathscr{S}}^{(e)} \frac{1}{k} \begin{bmatrix} n_x & 0 \\ 0 & n_y \\ n_y & n_x \end{bmatrix} - \begin{bmatrix} \partial_x \varphi^{(e)} & 0 \\ 0 & \partial_y \varphi^{(e)} \\ \partial_y \varphi^{(e)} & \partial_x \varphi^{(e)} \end{bmatrix}$$

where $\bigcup$ stands for the classical assembling operator and $\mathbf{n} = [n_x,\ n_y]^{\mathrm{T}}$.

Remark 2

Notice that matrices $\mathbf{B}^{(e)}$ and $\mathbf{B}^{*(e)}$ in Equation (25) differ in terms $\mathbf{G}^{(e)} \neq \mathbf{G}^{*(e)}$. This fact makes the resulting tangent stiffness matrix non-symmetrical as could be expected from the original non-symmetric character of the approach stated in Remark 1.

Remark 3

The structure of Equations (23)–(25) suggests the introduction of an internal additional fifth node for each element e that is activated only for the elements crossed by the discontinuity interface ($e \in \mathscr{J}$) and whose corresponding degrees of freedom and associated shape function are, respectively, the displacement jumps $[[\mathbf{u}]]_e$ and $\mathscr{M}_{\mathscr{S}}^{(e)}$ in Equations (11) and (12). Since the support of $\mathscr{M}_{\mathscr{S}}^{(e)}$ is only Ω_e, those internal degrees of freedom can be eventually condensed at the elemental level and removed from the global system of equations.

3. SYMMETRIC ASSUMED ENHANCED STRAIN APPROACH

The assumed enhanced strain methods, which can be considered a particular case of the more general assumed strain methods or mixed methods [23], provide a different setting to approach displacement discontinuities. In next sections the corresponding formulation is presented following the guidelines in Reference [24].

3.1. Assumed enhanced strain and stress fields

Let us consider the displacements $\mathbf{u}(\mathbf{x},t)$, enhanced strains $\tilde{\boldsymbol{\varepsilon}}(\mathbf{x},t)$ and stresses $\boldsymbol{\sigma}(\mathbf{x},t)$ to lie in the following functional spaces:

$$\mathscr{V}_{\mathbf{u}} \overset{\text{def}}{\equiv} \{\boldsymbol{\eta}(\mathbf{x}) \in [\mathsf{H}^1(\Omega)]^2\}$$

$$\mathscr{V}_{\mathbf{u}}^0 \overset{\text{def}}{\equiv} \{\boldsymbol{\eta}^0(\mathbf{x}) \in [\mathsf{H}^1(\Omega)]^2;\ \ \boldsymbol{\eta}^0|_{\partial_u\Omega} = \mathbf{0}\}$$

$$\mathscr{V}_{\tilde{\boldsymbol{\varepsilon}}} \overset{\text{def}}{\equiv} \{\tilde{\boldsymbol{\xi}}(\mathbf{x}) = \bar{\boldsymbol{\xi}} + \delta_{\mathscr{S}}(\boldsymbol{\alpha}\otimes\mathbf{n})^{\mathrm{S}}; \begin{cases} \bar{\xi}_{ij} \in \mathsf{L}_2(\Omega);\ \ \alpha_i \in \mathsf{L}_2(\mathscr{S}) \\ \displaystyle\int_\Omega \tilde{\boldsymbol{\xi}} : \boldsymbol{\tau}\, \mathrm{d}\Omega = 0 \quad \forall \boldsymbol{\tau} \in \mathscr{V}_{\boldsymbol{\sigma}} \end{cases} \tag{26}$$

$$\mathscr{V}_{\boldsymbol{\sigma}} \overset{\text{def}}{\equiv} \{\boldsymbol{\tau}(\mathbf{x});\ \ \tau_{ij} \in \mathsf{L}_2(\Omega)\}$$

where the orthogonality of $\mathscr{V}_{\tilde{\boldsymbol{\varepsilon}}}$ with respect $\mathscr{V}_{\boldsymbol{\sigma}}$ set through:

$$\int_\Omega \tilde{\boldsymbol{\xi}} : \boldsymbol{\tau}\, \mathrm{d}\Omega = 0 \quad \forall \tilde{\boldsymbol{\xi}} \in \mathscr{V}_{\tilde{\boldsymbol{\varepsilon}}} \quad \forall \boldsymbol{\tau} \in \mathscr{V}_{\boldsymbol{\sigma}} \tag{27}$$

is motivated by the satisfaction of the *patch test* [24].

The variational assumed enhanced strain problem can be written as:

Problem 3 (Continuous assumed enhanced strain problem)

Find

$$\dot{\mathbf{u}}(\mathbf{x},t); \qquad \dot{\mathbf{u}} \in \mathscr{V}_{\mathbf{u}} \tag{28a}$$

$$\left.\begin{aligned} \dot{\boldsymbol{\varepsilon}}(\mathbf{x},t) &= \nabla^{\mathrm{S}}\dot{\mathbf{u}} + \underbrace{\dot{\tilde{\boldsymbol{\varepsilon}}}}_{\text{enhanced part}} \\ \dot{\tilde{\boldsymbol{\varepsilon}}} &= \dot{\bar{\boldsymbol{\varepsilon}}} + \delta_s(\dot{\boldsymbol{\beta}}\otimes\mathbf{n})^{\mathrm{S}} \end{aligned}\right\}; \qquad \dot{\tilde{\boldsymbol{\varepsilon}}} \in \mathscr{V}_{\tilde{\boldsymbol{\varepsilon}}} \tag{28b}$$

$$\dot{\boldsymbol{\sigma}}(\mathbf{x},t); \qquad \dot{\boldsymbol{\sigma}} \in \mathscr{V}_{\boldsymbol{\sigma}} \tag{28c}$$

Such that

$$\delta\Pi_u(\dot{\boldsymbol{\Sigma}};\boldsymbol{\eta}) = \int_{\Omega\setminus\mathscr{S}} \dot{\boldsymbol{\Sigma}}(\boldsymbol{\varepsilon}) : \nabla^{\mathrm{S}}\boldsymbol{\eta}\, \mathrm{d}\Omega - G_{\text{ext}} = 0 \quad \forall \boldsymbol{\eta} \in \mathscr{V}_{\mathbf{u}}^0 \tag{29a}$$

$$\delta\Pi_{\tilde{\boldsymbol{\varepsilon}}}(\tilde{\boldsymbol{\varepsilon}};\boldsymbol{\tau}) = \int_\Omega \dot{\tilde{\boldsymbol{\varepsilon}}} : \boldsymbol{\tau}\, \mathrm{d}\Omega = 0 \qquad \forall \boldsymbol{\tau} \in \mathscr{V}_{\boldsymbol{\sigma}} \tag{29b}$$

$$\delta\Pi_\sigma(\dot{\boldsymbol{\sigma}},\dot{\boldsymbol{\Sigma}};\tilde{\boldsymbol{\xi}}) = \int_\Omega (\dot{\boldsymbol{\sigma}} - \dot{\boldsymbol{\Sigma}}) : \tilde{\boldsymbol{\xi}}\, \mathrm{d}\Omega = 0 \qquad \forall \tilde{\boldsymbol{\xi}} \in \mathscr{V}_{\tilde{\boldsymbol{\varepsilon}}} \tag{29c}$$

Remark 4

By comparison of the structure of the strain fields in Equations (1) and (28) the values $\boldsymbol{\beta}$, in the assumed strain field $\tilde{\boldsymbol{\varepsilon}}$, approach the displacement jumps $[[\mathbf{u}]]$ of the strong discontinuity kinematics (1).

Some standard calculations on Equations (29a–b) show that their strong forms are:

(i)

$$\delta\Pi_u(\dot{\boldsymbol{\Sigma}};\boldsymbol{\eta})=0 \;\Rightarrow\; \begin{cases} \nabla\cdot\dot{\boldsymbol{\Sigma}}(\boldsymbol{\varepsilon})-\dot{\mathbf{b}}=\mathbf{0} & \text{in } \Omega\backslash\mathscr{S} \\ \dot{\boldsymbol{\Sigma}}\cdot\boldsymbol{\nu}=\dot{\mathbf{t}} & \text{on } \partial_\sigma\Omega \\ [[\dot{\boldsymbol{\Sigma}}]]_{\Omega\backslash\mathscr{S}}\cdot\mathbf{n}=\mathbf{0} & \text{on } \mathscr{S} \end{cases} \tag{30}$$

(ii)

$$\delta\Pi_{\tilde{\varepsilon}}(\tilde{\boldsymbol{\varepsilon}};\boldsymbol{\tau})=0 \;\Rightarrow\; \int_\Omega \dot{\tilde{\boldsymbol{\varepsilon}}}:\boldsymbol{\tau}\,\mathrm{d}\Omega=0 \;\Rightarrow\; \dot{\tilde{\boldsymbol{\varepsilon}}}=0 \quad \text{in } \Omega \tag{31}$$

in a distributional sense[¶¶] and, in view of Equation (28b)

$$\dot{\boldsymbol{\varepsilon}}=\nabla^{\mathrm{S}}\dot{\mathbf{u}}+\underbrace{\dot{\tilde{\boldsymbol{\varepsilon}}}}_{=0}=\nabla^{\mathrm{S}}\dot{\mathbf{u}} \;\Rightarrow\; \dot{\boldsymbol{\varepsilon}}-\nabla^{\mathrm{S}}\dot{\mathbf{u}}=\mathbf{0} \quad \text{in } \Omega \tag{32}$$

Finally, Equation (29c) can be rewritten as

(iii)

$$\int_\Omega(\dot{\boldsymbol{\sigma}}-\dot{\boldsymbol{\Sigma}}):\tilde{\boldsymbol{\xi}}\,\mathrm{d}\Omega=\underbrace{\int_\Omega\dot{\boldsymbol{\sigma}}:\tilde{\boldsymbol{\xi}}\,\mathrm{d}\Omega}_{=0}-\int_\Omega\dot{\boldsymbol{\Sigma}}:\tilde{\boldsymbol{\xi}}\,\mathrm{d}\Omega=0 \tag{33}$$

$$\Rightarrow\int_\Omega\dot{\boldsymbol{\Sigma}}(\boldsymbol{\varepsilon}):\tilde{\boldsymbol{\xi}}\,\mathrm{d}\Omega=0 \tag{34}$$

Clearly Equations (29a) and (29b) are weak forms of Equations (4a)–(4d). Therefore $\tilde{\boldsymbol{\xi}}$ in Equation (34) has to be chosen to enforce the remaining Equation (4e).

3.2. Finite element discretization (standard constant stress/enhanced strain element: S4n)

Given a finite element discretization in four-noded elements (see Figure 2(a)), let us consider the following discrete version of the spaces in Equation (26):

$$\begin{aligned} \mathscr{V}_{\mathbf{u}}^{\mathrm{h}} &\overset{\text{def}}{\equiv} \left\{\boldsymbol{\eta}^{\mathrm{h}}(\mathbf{x})=\sum_{i=1}^{i=n_{\text{node}}}N_i(\mathbf{x})\boldsymbol{\eta}_i\right\} \\ \mathscr{V}_{\mathbf{u}}^{\mathrm{h}^0} &\overset{\text{def}}{\equiv} \left\{\boldsymbol{\eta}^{\mathrm{h}}(\mathbf{x})=\sum_{i=1}^{i=n_{\text{node}}}N_i(\mathbf{x})\boldsymbol{\eta}_i;\;\; \boldsymbol{\eta}_i|_{\partial_u\Omega}=\mathbf{0}\right\} \\ \mathscr{V}_{\tilde{\boldsymbol{\varepsilon}}}^{\mathrm{h}} &\equiv \left\{\tilde{\boldsymbol{\xi}}^{\mathrm{h}}(\mathbf{x})=\sum_{e=1}^{e=n_{\text{elem}}}\left(\mu_{\mathscr{S}}^{(e)}\frac{1}{k}-\frac{l_e}{\Omega_e}\right)\chi_e(\mathbf{x})(\boldsymbol{\alpha}_e\otimes\mathbf{n})^{\mathrm{S}}\right\},\;\; \chi_e(\mathbf{x})=\begin{cases}1 & \text{for } \mathbf{x}\in\Omega_e\\ 0 & \text{otherwise}\end{cases} \end{aligned} \tag{35}$$

[¶¶] Since, from Equation (28), $\dot{\tilde{\boldsymbol{\varepsilon}}}=\dot{\tilde{\boldsymbol{\varepsilon}}}+\delta_s(\dot{\boldsymbol{\beta}}\otimes\mathbf{n})^{\mathrm{S}}$ is a distribution, the expression $\dot{\tilde{\boldsymbol{\varepsilon}}}=\mathbf{0}$ has to be understood in the distributional sense.

$$\mathscr{V}_{\boldsymbol{\sigma}}^{\mathrm{h}} \overset{\text{def}}{\equiv} \left\{ \boldsymbol{\tau}^{\mathrm{h}}(\mathbf{x}) = \sum_{e=1}^{e=n_{\text{elem}}} \chi_e(\mathbf{x}) \tau_e \right\}$$

It can be immediately noticed that the chosen expansions for the discrete assumed strain field $\tilde{\boldsymbol{\xi}}^{\mathrm{h}}$ in Equation (35) fulfil the orthogonality condition (27) since

$$\begin{aligned} \int_{\Omega} \tilde{\boldsymbol{\xi}}^{\mathrm{h}} : \boldsymbol{\tau}^{\mathrm{h}} \, \mathrm{d}\Omega &= \sum_{e=1}^{e=n_{\text{elem}}} \int_{\Omega_e} \left(\mu_{\mathscr{S}}^{(e)} \frac{1}{k} - \frac{l_e}{\Omega_e} \right) (\boldsymbol{\alpha}_e \otimes \mathbf{n})^{\mathrm{S}} : \tau_e \, \mathrm{d}\Omega \\ &= \sum_{e=1}^{e=n_{\text{elem}}} \underbrace{\int_{\Omega_e} \left(\mu_{\mathscr{S}}^{(e)} \frac{1}{k} - \frac{l_e}{\Omega_e} \right) \mathrm{d}\Omega}_{(l_e - l_e) = 0} (\boldsymbol{\alpha}_e \otimes \mathbf{n})^{\mathrm{S}} : \tau_e = 0 \end{aligned} \tag{36}$$

In this context the discrete counterpart of the continuum Problem 3 in Equation (28) to (29) reads:

Problem 4 (*Discrete assumed enhanced strain problem*)

Find

$$\begin{aligned} &\dot{\mathbf{u}}^{\mathrm{h}}(\mathbf{x}, t) = \sum_{i=1}^{i=n_{\text{node}}} N_i \dot{\mathbf{d}}_i, && \dot{\mathbf{u}}^{\mathrm{h}} \in \mathscr{V}_{\mathbf{u}}^{\mathrm{h}} \\ &\dot{\boldsymbol{\varepsilon}}^{\mathrm{h}}(\mathbf{x}, t) = \nabla^{\mathrm{S}} \mathbf{u}^{\mathrm{h}} + \underbrace{\sum_{e=1}^{e=n_{\text{elem}}} \left(\mu_{\mathscr{S}}^{(e)} \frac{1}{k} - \frac{l_e}{\Omega_e} \right) \chi_e(\mathbf{x}) (\dot{\boldsymbol{\beta}}_e \otimes \mathbf{n})^{\mathrm{S}}}_{\dot{\tilde{\boldsymbol{\varepsilon}}}^{\mathrm{h}} (\text{enhancement})} && \dot{\tilde{\boldsymbol{\varepsilon}}}^{\mathrm{h}} \in \mathscr{V}_{\tilde{\boldsymbol{\varepsilon}}}^{\mathrm{h}} \\ &\dot{\boldsymbol{\sigma}}^{\mathrm{h}}(\mathbf{x}, t) = \sum_{e=1}^{e=n_{\text{elem}}} \chi_e(\mathbf{x}) \dot{\boldsymbol{\sigma}}_e && \dot{\boldsymbol{\sigma}}^{\mathrm{h}} \in \mathscr{V}_{\boldsymbol{\sigma}}^{\mathrm{h}} \end{aligned} \tag{37}$$

Such that

(i)

$$\delta \Pi_u(\dot{\boldsymbol{\Sigma}}; \boldsymbol{\eta}^{\mathrm{h}}) = 0 \;\Rightarrow\; \sum_{e=1}^{e=n_{\text{elem}}} \int_{\Omega_e} \nabla^{\mathrm{S}} \boldsymbol{\eta}^{\mathrm{h}} : \dot{\boldsymbol{\Sigma}}(\boldsymbol{\varepsilon}^{\mathrm{h}}) \, \mathrm{d}\Omega - G_{\text{ext}} = 0 \quad \forall \boldsymbol{\eta}^{\mathrm{h}} \in \mathscr{V}_{\mathbf{u}}^{0} \tag{38}$$

(ii)

$$\delta \Pi_{\tilde{\varepsilon}}(\tilde{\boldsymbol{\varepsilon}}^{\mathrm{h}}; \boldsymbol{\varepsilon}^{\mathrm{h}}) = 0 \;\Rightarrow\; (\text{trivially fulfilled, see Equation (36)}) \tag{39}$$

(iii)

$$\delta \Pi_{\sigma}(\dot{\boldsymbol{\sigma}}^{\mathrm{h}}, \dot{\boldsymbol{\Sigma}}; \tilde{\boldsymbol{\tau}}^{\mathrm{h}}) = \mathbf{0} \;\Rightarrow\; \begin{cases} \sum_{e=1}^{e=n_{\text{elem}}} \displaystyle\int_{\Omega_e} \dot{\boldsymbol{\Sigma}} : \tilde{\boldsymbol{\tau}}^{\mathrm{h}} \, \mathrm{d}\Omega \\ \quad = \sum_{e=1}^{e=n_{\text{elem}}} \left[\displaystyle\int_{\Omega_e} \left(\mu_{\mathscr{S}}^{(e)} \frac{1}{k} - \frac{l_e}{\Omega_e} \right) \dot{\boldsymbol{\Sigma}} \cdot \mathbf{n} \, \mathrm{d}\Omega \right] \cdot \alpha_e = 0 \quad \forall \alpha_e \end{cases} \tag{40}$$

$$\Rightarrow \int_{\Omega_e} \left(\mu_{\mathscr{S}}^{(e)} \frac{1}{k} - \frac{l_e}{\Omega_e} \right) \dot{\boldsymbol{\Sigma}} \cdot \mathbf{n} \, \mathrm{d}\Omega = \mathbf{0} \quad e \in \{1 \ldots n_{\text{elem}}\} \tag{41}$$

Remark 5
Equation (41) can be rewritten as

$$\int_{\Omega_e}\left(\mu_{\mathscr{S}}^{(e)}\frac{1}{kl_e}-\frac{1}{\Omega_e}\right)\dot{\boldsymbol{\Sigma}}\cdot\mathbf{n}\,\mathrm{d}\Omega=\mathbf{0}\Rightarrow$$
$$\underbrace{\frac{1}{\Omega_e}\int_{\Omega_e}\dot{\boldsymbol{\Sigma}}\,\mathrm{d}\Omega}_{\overline{\dot{\boldsymbol{\Sigma}}}_{\Omega_e}\ \text{(average in }\Omega_e)}\cdot\mathbf{n}=\underbrace{\frac{1}{l_e}\int_{l_e}\dot{\boldsymbol{\Sigma}}\,\mathrm{d}\mathscr{S}}_{\overline{\dot{\boldsymbol{\Sigma}}}_{\mathscr{S}_e}\ \text{(average in }\mathscr{S}_e)}\cdot\mathbf{n}\ \Rightarrow\ \underbrace{\overline{\dot{\boldsymbol{\Sigma}}}_{\Omega_e}\cdot\mathbf{n}=\overline{\dot{\boldsymbol{\Sigma}}}_{\mathscr{S}_e}\cdot\mathbf{n}}_{\boldsymbol{\Sigma}\ \text{traction continuity (in mean values)}}\tag{42}$$

which shows that Equation (41) is imposing the inner $\boldsymbol{\Sigma}$ traction continuity inside every element.

In summary, the equations ruling the discrete symmetric problem (4) can be written as

$$\left.\begin{aligned}\delta\Pi_u(\dot{\boldsymbol{\Sigma}};\boldsymbol{\eta}^{\mathrm{h}})&=0\\ \delta\Pi_\sigma(\dot{\boldsymbol{\sigma}}^{\mathrm{h}},\dot{\boldsymbol{\Sigma}};\tilde{\boldsymbol{\xi}}^{\mathrm{h}})&=0\end{aligned}\right\}\Rightarrow\begin{cases}\bigcup\limits_{e=1}^{e=n_{\mathrm{elem}}}\displaystyle\int_{\Omega_e}\nabla^{\mathrm{S}}\boldsymbol{\eta}^{\mathrm{h}}:\dot{\boldsymbol{\Sigma}}(\boldsymbol{\varepsilon})\,\mathrm{d}\Omega-G_{\mathrm{ext}}=0 & \forall\boldsymbol{\eta}^{\mathrm{h}}\in\mathscr{V}_{\mathbf{u}}^{0}\\ \displaystyle\int_{\Omega_e}\left(\mu_{\mathscr{S}}^{(e)}\frac{1}{k}-\frac{l_e}{\Omega_e}\right)\cdot\mathbf{n}\cdot\dot{\boldsymbol{\Sigma}}\,\mathrm{d}\Omega=\mathbf{0} & e\in\{1\ldots n_{\mathrm{elem}}\}\end{cases}\tag{43}$$

$$\dot{\boldsymbol{\varepsilon}}^{(e)}=\nabla^{\mathrm{S}}\dot{\mathbf{u}}^{(e)}+\left(\mu_{\mathscr{S}}^{(e)}\frac{1}{k}-\frac{l_e}{\Omega_e}\right)(\dot{\boldsymbol{\beta}}_e\otimes\mathbf{n})^{\mathrm{S}}\tag{44}$$

3.2.1. 2D implementation. For the two-dimensional case, considering the four-noded quadrilateral as underlaying element and the finite element *B-format*, Equations (43) and (44) yield to the symmetric system of equations:

$$\left.\begin{aligned}\delta\Pi_u(\dot{\boldsymbol{\Sigma}};\boldsymbol{\eta}^{\mathrm{h}})&=0\\ \delta\Pi_\sigma(\dot{\boldsymbol{\sigma}}^{\mathrm{h}},\dot{\boldsymbol{\Sigma}};\tilde{\boldsymbol{\xi}}^{\mathrm{h}})&=0\end{aligned}\right\}\Rightarrow\bigcup_{e=1}^{e=n_{\mathrm{elem}}}\left[\int_{\Omega_e}\mathbf{B}^{(e)^{\mathrm{T}}}\cdot\{\dot{\Sigma}\}\,\mathrm{d}\Omega-\dot{\mathbf{F}}^{\mathrm{ext}(e)}\right]=\mathbf{0}\tag{45}$$

$$\begin{aligned}\{\dot{\varepsilon}\}^{(e)}&=\mathbf{B}^{(e)}\cdot\dot{\mathbf{d}}^{(e)}\\ \dot{\mathbf{d}}^{(e)}&=[\dot{\mathbf{d}}_1,\ \dot{\mathbf{d}}_2,\ \dot{\mathbf{d}}_3,\ \dot{\mathbf{d}}_4,\ \dot{\boldsymbol{\beta}}_e]^{\mathrm{T}}\\ \mathbf{B}^{(e)}&=[\mathbf{B}_1^{(e)},\ \mathbf{B}_2^{(e)},\ \mathbf{B}_3^{(e)},\ \mathbf{B}_4^{(e)},\ \mathbf{G}^{(e)}]\end{aligned}\tag{46}$$

$$\begin{aligned}\mathbf{B}_i^{(e)}&=\begin{bmatrix}\partial_x N_i^{(e)} & 0\\ 0 & \partial_y N_i^{(e)}\\ \partial_y N_i^{(e)} & \partial_x N_i^{(e)}\end{bmatrix}\\ \mathbf{G}^{(e)}&=\left(\mu_{\mathscr{S}}^{(e)}\frac{1}{k}-\frac{l_e}{\Omega_e}\right)\begin{bmatrix}n_x & 0\\ 0 & n_y\\ n_y & n_x\end{bmatrix}\end{aligned}\tag{47}$$

As in the non-symmetric element (see Remark 3), the degrees of freedom, $\boldsymbol{\beta}_e$, in Equation (46) can be tackled as an internal element fifth node (incompatible mode [24]), condensed at the elemental level and removed from the global system of equations.

4. NUMERICAL EXPERIMENT. STRESS LOCKING PHENOMENA

In order to check the performance of the elements previously described in Sections 2 and 3 the simple numerical test described in Figure 3(a) has been considered. A rectangular plate, modelled in plane strain, is fixed at one side and uniformly stretched from the other side. The material is modelled using the simple isotropic continuum damage model described in Reference [25] and equipped with linear softening. The theoretical analysis shows a solution for the problem consisting of a straight vertical discontinuity line crossing the plate from the top to the bottom. The displacement jump is uniform and exhibits only a normal component.

Since the problem is homogeneous before bifurcation, the stress state is constant and the position of the discontinuity line is not determined. For the purposes of the analysis, this position is artificially fixed.

The numerical simulation is carried out using an arbitrary oriented mesh, as shown in Figure 3(a), with the following finite elements:

- *Standard non-symmetric four-noded element U4n*. This is the non-symmetrical statically and kinematically consistent element based on the Petrov–Galerkin approach described in Section 2.
- *Standard symmetric four-noded element S4n*. This is the symmetric statically consistent element based on the assumed enhanced strain approach described in Section 3.

In Figure 3(b) the obtained stress–displacement curves, σ_{xx}–δ, for both elements are plotted. It can be readily checked that the *U4n* element provides the expected *exact* solution exhibiting, beyond the peak stress, a linear softening branch up to the total stress relaxation.

The S4n element, instead, exhibits a hardening branch beyond the theoretical peak, that rises the stress–displacement curve up to unphysical levels.

A deeper look at the numerical results shows that this unexpected structural hardening comes out from the fact that material points at $\Omega \backslash \mathscr{S}$ which are supposed to behave elastically after

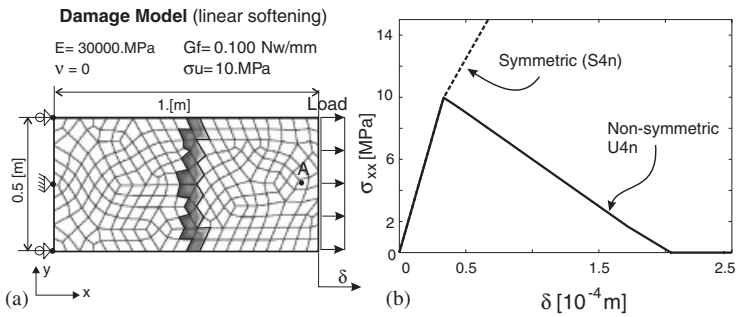

Figure 3. Homogeneous plate: (a) geometrical data and finite element mesh; and (b) stress σ_{xx} (at point A) vs displacement δ curves.

the bifurcation, do not unload but, instead, load elastically after bifurcation.[|||] This results in the unexpectedly high stress levels observed in the figure. This trend is not modified by using finer meshes, and therefore, convergence to the exact solution is not achieved with mesh refinement. Clearly this is a typical stress-locking behaviour that actually makes the S4n element unsuitable for any modelling purposes.

In order to look for remedies for this stress locking, its causes are analysed through the following reasonings:

1. The strong discontinuity kinematics in Equation (1) splits the strains into a regular (bounded) part that develops at $\Omega/\mathscr{S}$ and a singular (unbounded) part that develops at $\mathscr{S}$

$$\dot{\boldsymbol{\varepsilon}} = \nabla^{\mathrm{S}}\dot{\mathbf{u}} = \underbrace{\dot{\bar{\boldsymbol{\varepsilon}}}}_{\substack{\dot{\varepsilon}_{\Omega\setminus\mathscr{S}} \\ \text{regular (bounded)}}} + \underbrace{\delta_{\mathscr{S}}(\llbracket\dot{\mathbf{u}}\rrbracket \otimes \mathbf{n})^{\mathrm{S}}}_{\text{singular (unbounded)}} \tag{48}$$

2. It can be shown that, after the onset of the strong discontinuity, the whole inelastic (rate of) strain component matches the singular part whereas the regular (rate of) strain remains incrementally elastic[***] i.e.:

$$\dot{\boldsymbol{\varepsilon}}_{\Omega\setminus\mathscr{S}} = \dot{\bar{\boldsymbol{\varepsilon}}} = \underbrace{\mathbf{C}^{-1} : \dot{\boldsymbol{\sigma}}}_{\text{elastic strain}} \;\Rightarrow\; \dot{\boldsymbol{\sigma}} = \mathbf{C} : \dot{\boldsymbol{\varepsilon}}_{\Omega\setminus\mathscr{S}} \tag{49}$$

   where $\mathbf{C}$ stands for the elastic fourth-order constitutive tensor.
3. A glance at Equation (49) shows that, since the components of $\mathbf{C}$ (determined by the normally high values of the elastic properties) are very large, the values of $\dot{\boldsymbol{\varepsilon}}_{\Omega\setminus\mathscr{S}}$ have to be very small for $\dot{\sigma}$ to be in the physically expected range. In other words, if the values of $\dot{\boldsymbol{\varepsilon}}_{\Omega\setminus\mathscr{S}}$ are unexpectedly large so will be the values of $\dot{\sigma}$, thus provoking *locking phenomena*. As a particular case, at the final stages of the stress–displacement curve in Figure 3(b) one can expect the regular strain to be practically zero.[†††]

$$\dot{\sigma} \simeq 0 \;\Rightarrow\; \dot{\boldsymbol{\varepsilon}}_{\Omega\setminus\mathscr{S}} = \mathbf{C}^{-1} : \dot{\sigma} \simeq 0 \tag{50}$$

   Now, looking at the elemental strain field modelled by the *S4n* element (see Equation (37)) and the polynomial degree of its counterparts:

$$\dot{\boldsymbol{\varepsilon}}^{(e)}_{\Omega\setminus\mathscr{S}} = \underbrace{\nabla^{\mathrm{S}}\dot{\mathbf{u}}^{(e)}}_{\text{linear}} - \underbrace{\frac{l_e}{\Omega_e}(\dot{\boldsymbol{\beta}}_e \otimes \mathbf{n})^{\mathrm{S}}}_{\text{(enhancement) constant}} \tag{51}$$

   we realize that, except for very particular cases in which the term $\nabla^{\mathrm{S}}\dot{\mathbf{u}}^{(e)}$ becomes constant inside the element, for the very general case both terms will not cancel each other. Thus, Equation (50) will not be fulfilled and stress locking will arise.

[|||] This theoretical incrementally elastic behaviour is algorithmically imposed at the bulk $\Omega\setminus\mathscr{S}$ after bifurcation.

[***] Though intuitive this is not a trivial result. Its proof requires resorting to the so-called strong discontinuity analysis [25].

[†††] At this stage, the element should be able to produce rigid body motions of the two portions split up by the discontinuity at no stress and, therefore, at no elastic strain.

These arguments explain, at least crudely, the reasons for the locking phenomena observed in element S4n and also suggest two possible strategies as remedies:

(a) Decrease the polynomial degree of the term $\nabla^{\mathrm{S}}\dot{\mathbf{u}}^{(e)}$ to zero (constant).
(b) Increase the polynomial degree of the enhancement term to one (linear polynomial).

Strategy (a) is followed in the mixed approach presented in Section 5 whereas strategy (b) leads to the strain re-enhancement methodology presented in Section 6.[‡‡‡]

5. MIXED APPROACH

5.1. Assumed strain and stress fields

Let us consider the following functional spaces:

$$\mathscr{V}_{\mathbf{u}} \overset{\text{def}}{\equiv} \{\boldsymbol{\eta}(\mathbf{x}) \in [\mathsf{H}^1(\Omega)]^2\} \tag{52a}$$

$$\mathscr{V}_{\mathbf{u}}^0 \overset{\text{def}}{\equiv} \{\boldsymbol{\eta}^0(\mathbf{x}) \in [\mathsf{H}^1(\Omega)]^2; \boldsymbol{\eta}^0|_{\partial_u\Omega} = \mathbf{0}\} \tag{52b}$$

$$\mathscr{V}_{\boldsymbol{\varepsilon}} \overset{\text{def}}{\equiv} \{\boldsymbol{\xi}(\mathbf{x}) = \bar{\boldsymbol{\xi}} + \delta_{\mathscr{S}}(\boldsymbol{\alpha} \otimes \mathbf{n})^{\mathrm{S}}; \bar{\boldsymbol{\xi}}_{ij} \in L_2(\Omega); \alpha_i \in \mathsf{L}_2(\mathscr{S})\} \tag{52c}$$

$$\mathscr{V}_{\boldsymbol{\sigma}} \overset{\text{def}}{\equiv} \{\boldsymbol{\tau}(\mathbf{x}); \tau_{ij} \in \mathsf{L}_2(\Omega);\ [[\boldsymbol{\tau}]]_{\Omega\setminus\mathscr{S}} \cdot \mathbf{n} = [[\boldsymbol{\tau}]]_{\mathscr{S}} \cdot \mathbf{n} = \mathbf{0}\} \tag{52d}$$

The variational three field ($\mathbf{u}$–$\boldsymbol{\varepsilon}$–$\boldsymbol{\sigma}$) mixed problem can we written as

Problem 5 (*Continuous mixed problem*)

Find

$$\begin{aligned} &\dot{\mathbf{u}}(\mathbf{x}, t) && \dot{\mathbf{u}} \in \mathscr{V}_{\mathbf{u}} \\ &\dot{\boldsymbol{\varepsilon}}(\mathbf{x}, t) = \dot{\bar{\boldsymbol{\varepsilon}}} + \delta_s(\dot{\boldsymbol{\beta}} \otimes \mathbf{n})^{\mathrm{S}} && \dot{\boldsymbol{\varepsilon}} \in \mathscr{V}_{\boldsymbol{\varepsilon}} \\ &\dot{\boldsymbol{\sigma}}(\mathbf{x}, t) && \dot{\boldsymbol{\sigma}} \in \mathscr{V}_{\boldsymbol{\sigma}} \end{aligned} \tag{53}$$

Such that

$$\begin{aligned} \delta\Pi_u(\dot{\boldsymbol{\sigma}}; \boldsymbol{\eta}) &= \int_{\Omega\setminus\mathscr{S}} \dot{\boldsymbol{\sigma}} : \nabla^{\mathrm{S}}\boldsymbol{\eta}\, \mathrm{d}\Omega - G_{\mathrm{ext}} = 0 \qquad \forall \boldsymbol{\eta} \in \mathscr{V}_{\mathbf{u}}^0 \\ \delta\Pi_{\boldsymbol{\varepsilon}}(\dot{\mathbf{u}}, \dot{\boldsymbol{\varepsilon}}; \boldsymbol{\tau}) &= \int_{\Omega} (\dot{\boldsymbol{\varepsilon}} - \nabla^{\mathrm{S}}\dot{\mathbf{u}}) : \boldsymbol{\tau}\, \mathrm{d}\Omega = 0 \qquad \forall \boldsymbol{\tau} \in \mathscr{V}_{\boldsymbol{\sigma}} \\ \delta\Pi_{\sigma}(\dot{\boldsymbol{\sigma}}, \dot{\boldsymbol{\Sigma}}; \boldsymbol{\xi}) &= \int_{\Omega} (\dot{\boldsymbol{\sigma}} - \dot{\boldsymbol{\Sigma}}) : \boldsymbol{\xi}\, \mathrm{d}\Omega = 0 \quad \forall \boldsymbol{\xi} \in \mathscr{V}_{\boldsymbol{\varepsilon}} \end{aligned} \tag{54}$$

[‡‡‡]Indeed, these strategies for alleviating the stress-locking problem can only be applied to finite elements sensitive to mixed/assumed strain or assumed enhanced strain technologies, like the four-noded quadrilateral. For instance, strategies (a) and (b) cannot be applied, at elemental level, to linear triangles.

Standard calculations on Equations (54) lead to the corresponding strong forms:

(i)

$$\delta\Pi_u(\dot{\boldsymbol{\sigma}};\boldsymbol{\eta})=0 \;\Rightarrow\; \begin{cases} \nabla\cdot\dot{\boldsymbol{\sigma}}+\dot{\mathbf{b}}=\mathbf{0} & \text{in } \Omega\backslash\mathscr{S} \\ \dot{\boldsymbol{\sigma}}\cdot\boldsymbol{\nu}=\dot{\mathbf{t}} & \text{on } \partial_\sigma\Omega \\ [[\dot{\boldsymbol{\sigma}}]]_{\Omega\backslash\mathscr{S}}\cdot\mathbf{n}=\mathbf{0} & \text{on } \mathscr{S} \end{cases} \tag{55}$$

(ii)

$$\delta\Pi_e(\dot{\mathbf{u}},\dot{\boldsymbol{\varepsilon}};\boldsymbol{\tau})=0 \;\Rightarrow\; \int_\Omega(\dot{\boldsymbol{\varepsilon}}-\nabla^{\mathrm{S}}\dot{\mathbf{u}}):\boldsymbol{\tau}\,\mathrm{d}\Omega=0 \;\Rightarrow\; \dot{\boldsymbol{\varepsilon}}=\nabla^{\mathrm{S}}\dot{\mathbf{u}} \quad \text{in } \Omega \tag{56}$$

(iii)

$$\delta\Pi_\sigma(\dot{\boldsymbol{\sigma}},\dot{\boldsymbol{\Sigma}};\boldsymbol{\xi})=0 \;\Rightarrow\; \int_\Omega(\dot{\boldsymbol{\sigma}}-\dot{\boldsymbol{\Sigma}}):\boldsymbol{\xi}\,\mathrm{d}\Omega \;\Rightarrow\; \dot{\boldsymbol{\sigma}}=\dot{\boldsymbol{\Sigma}} \quad \text{in } \Omega \tag{57}$$

Therefore, Equations (3a)–(3e) of the original BVP are fulfilled in weak form by the variational Equations (54) whereas Equation (3f) is fulfilled from the particular choice made for the space $\mathscr{V}_{\boldsymbol{\sigma}}$ in Equation (52d).

5.2. *Finite element discretization (constant stress/strain mixed element: M4n)*

For the four-noded element discretization of Figure 2(a) let us consider the following discrete counterpart of the spaces in Equation (52):

$$\mathscr{V}_{\mathbf{u}}^{\mathrm{h}} \overset{\mathrm{def}}{\equiv} \left\{ \boldsymbol{\eta}^{\mathrm{h}}(\mathbf{x})=\sum_{i=1}^{i=n_{\mathrm{node}}} N_i(\mathbf{x})\boldsymbol{\eta}_i \right\} \tag{58a}$$

$$\mathscr{V}_{\mathbf{u}}^{0} \overset{\mathrm{def}}{\equiv} \left\{ \boldsymbol{\eta}^{\mathrm{h}}(\mathbf{x})=\sum_{i=1}^{i=n_{\mathrm{node}}} N_i(\mathbf{x})\boldsymbol{\eta}_i;\;\; \boldsymbol{\eta}_i|_{\partial_u\Omega}=\mathbf{0} \right\} \tag{58b}$$

$$\mathscr{V}_{\boldsymbol{\varepsilon}}^{\mathrm{h}} \overset{\mathrm{def}}{\equiv} \left\{ \boldsymbol{\xi}^{\mathrm{h}}(\mathbf{x})=\sum_{e=1}^{e=n_{\mathrm{elem}}} \chi_e(\mathbf{x})\left(\bar{\boldsymbol{\xi}}_e+\mu_{\mathscr{S}}^{(e)}\frac{1}{k}(\boldsymbol{\alpha}_e\otimes\mathbf{n})^{\mathrm{S}}\right) \right\}; \quad \chi_e(\mathbf{x})=\begin{cases} 1 & \text{for } \mathbf{x}\in\Omega_e \\ 0 & \text{otherwise} \end{cases} \tag{58c}$$

$$\mathscr{V}_{\boldsymbol{\sigma}}^{\mathrm{h}} \overset{\mathrm{def}}{\equiv} \left\{ \boldsymbol{\tau}^{\mathrm{h}}P(\mathbf{x})=\sum_{e=1}^{e=n_{\mathrm{elem}}} \chi_e(\mathbf{x})\tau_e \right\} \tag{58d}$$

and the corresponding discrete problem:

Problem 6 (*Discrete mixed problem*)

Find

$$\dot{\mathbf{u}}^{\mathrm{h}}=\sum_{i=1}^{i=n_{\mathrm{node}}} N_i\dot{\mathbf{d}}_i; \qquad \dot{\mathbf{u}}^{\mathrm{h}}\in\mathscr{V}_{\mathbf{u}}^{\mathrm{h}} \tag{59a}$$

$$\dot{\boldsymbol{\varepsilon}}^{\mathrm{h}} = \sum_{e=1}^{e=n_{\mathrm{elem}}} \left(\chi_e(\mathbf{x}) \dot{\bar{\boldsymbol{\varepsilon}}}_e + \mu_{\mathscr{S}}^{(e)} \frac{1}{k} \chi_e(\mathbf{x}) (\dot{\boldsymbol{\beta}}_e \otimes \mathbf{n})^{\mathrm{S}} \right) \quad \dot{\boldsymbol{\varepsilon}}^{\mathrm{h}} \in \mathscr{V}_{\boldsymbol{\varepsilon}} \tag{59b}$$

$$\dot{\boldsymbol{\sigma}}^{\mathrm{h}} = \sum_{e=1}^{e=n_{\mathrm{elem}}} \chi_e(\mathbf{x}) \dot{\boldsymbol{\sigma}}_e \qquad \dot{\boldsymbol{\sigma}}^{\mathrm{h}} \in \mathscr{V}_{\boldsymbol{\sigma}} \tag{59c}$$

Such that

$$\delta \Pi_u(\dot{\boldsymbol{\sigma}}; \boldsymbol{\eta}^{\mathrm{h}}) = \int_\Omega \dot{\boldsymbol{\sigma}}^{\mathrm{h}} : \nabla^{\mathrm{S}} \boldsymbol{\eta}^{\mathrm{h}} \, \mathrm{d}\Omega - G_{\mathrm{ext}} = 0 \quad \forall \boldsymbol{\eta}^{\mathrm{h}} \in \mathscr{V}_{\mathbf{u}}^{\mathrm{h}^0} \tag{60a}$$

$$\delta \Pi_{\boldsymbol{\varepsilon}}(\dot{\mathbf{u}}^{\mathrm{h}}, \dot{\boldsymbol{\varepsilon}}^{\mathrm{h}}; \boldsymbol{\tau}^{\mathrm{h}}) = \int_\Omega (\dot{\boldsymbol{\varepsilon}}^{\mathrm{h}} - \nabla^{\mathrm{S}} \dot{\mathbf{u}}^{\mathrm{h}}) : \boldsymbol{\tau}^{\mathrm{h}} \, \mathrm{d}\Omega = 0 \quad \forall \boldsymbol{\tau}^{\mathrm{h}} \in \mathscr{V}_{\boldsymbol{\sigma}}^{\mathrm{h}} \tag{60b}$$

$$\delta \Pi_\sigma(\dot{\boldsymbol{\sigma}}^{\mathrm{h}}, \dot{\boldsymbol{\Sigma}}^{\mathrm{h}}; \boldsymbol{\xi}^{\mathrm{h}}) = \int_\Omega (\dot{\boldsymbol{\sigma}}^{\mathrm{h}} - \dot{\boldsymbol{\Sigma}}^{\mathrm{h}}) : \boldsymbol{\xi}^{\mathrm{h}} \, \mathrm{d}\Omega = 0 \quad \forall \boldsymbol{\xi}^{\mathrm{h}} \in \mathscr{V}_{\boldsymbol{\varepsilon}}^{\mathrm{h}} \tag{60c}$$

By inserting the strain rate field $\dot{\boldsymbol{\varepsilon}}^{\mathrm{h}}$ of Equation (59b) into Equation (60b) one gets

$$\begin{aligned} \delta \Pi_\varepsilon(\dot{\mathbf{u}}^{\mathrm{h}}, \dot{\boldsymbol{\varepsilon}}^{\mathrm{h}}) = 0 \Rightarrow & \sum_{e=1}^{e=n_{\mathrm{elem}}} \int_{\Omega_e} (\dot{\boldsymbol{\varepsilon}}^{\mathrm{h}} - \nabla^{\mathrm{S}} \dot{\mathbf{u}}^{\mathrm{h}}) : \boldsymbol{\tau}_e \, \mathrm{d}\Omega \\ & = \sum_{e=1}^{e=n_{\mathrm{elem}}} \left(\Omega_e \dot{\bar{\boldsymbol{\varepsilon}}}_e + l_e (\dot{\boldsymbol{\beta}}_e \otimes \mathbf{n})^{\mathrm{S}} - \int_{\Omega_e} \nabla^{\mathrm{S}} \dot{\mathbf{u}}^{\mathrm{h}} \, \mathrm{d}\Omega \right) \boldsymbol{\tau}_e = 0 \quad \forall \boldsymbol{\tau}_e \\ & \Rightarrow \left(\Omega_e \dot{\bar{\boldsymbol{\varepsilon}}}_e + l_e (\dot{\boldsymbol{\beta}}_e \otimes \mathbf{n})^{\mathrm{S}} - \int_{\Omega_e} \nabla^{\mathrm{S}} \dot{\mathbf{u}}^{\mathrm{h}} \, \mathrm{d}\Omega \right) = 0 \quad e \in \{1 \ldots n_{\mathrm{elem}}\} \Rightarrow \end{aligned} \tag{61}$$

and solving for $\dot{\bar{\boldsymbol{\varepsilon}}}_e$ and, then, for $\dot{\bar{\boldsymbol{\varepsilon}}}^{\mathrm{h}}$ in Equation (59b), we get

$$\begin{aligned} \dot{\bar{\boldsymbol{\varepsilon}}}_e &= \frac{1}{\Omega_e} \int_{\Omega_e} \nabla^{\mathrm{S}} \dot{\mathbf{u}}^{\mathrm{h}} \, \mathrm{d}\Omega - \frac{l_e}{\Omega_e} (\dot{\boldsymbol{\beta}}_e \otimes \mathbf{n})^{\mathrm{S}} \quad e \in \{1 \ldots n_{\mathrm{elem}}\} \Rightarrow \\ \dot{\bar{\boldsymbol{\varepsilon}}}^{\mathrm{h}} &= \sum_{e=1}^{e=n_{\mathrm{elem}}} \chi_e(\mathbf{x}) \left(\underbrace{\frac{1}{\Omega_e} \int_{\Omega_e} \nabla^{\mathrm{S}} \dot{\mathbf{u}}^{\mathrm{h}} \, \mathrm{d}\Omega}_{\stackrel{\mathrm{def}}{=} \overline{\nabla^{\mathrm{S}} \dot{\mathbf{u}}}^{(e)}} - \left(\frac{l_e}{\Omega_e} - \mu_{\mathscr{S}}^{(e)} \frac{1}{k} \right) (\dot{\boldsymbol{\beta}}_e \otimes \mathbf{n})^{\mathrm{S}} \right) \end{aligned} \tag{62}$$

where $\overline{\nabla^{\mathrm{S}} \dot{\mathbf{u}}}^{(e)}$ stands for the mean value of $\nabla^{\mathrm{S}} \dot{\mathbf{u}}^{\mathrm{h}}(\mathbf{x})$ inside the element e. In summary,

$$\delta \Pi_\varepsilon(\dot{\mathbf{u}}^{\mathrm{h}}, \dot{\boldsymbol{\varepsilon}}^{\mathrm{h}} : \boldsymbol{\tau}^{\mathrm{h}}) = 0 \rightarrow \dot{\boldsymbol{\varepsilon}}^{\mathrm{h}} = \sum_{e=1}^{e=n_{\mathrm{elem}}} \chi_e(\mathbf{x}) \left[\overline{\nabla^{\mathrm{S}} \dot{\mathbf{u}}}^{(e)} + \left(\mu_{\mathscr{S}}^{(e)} \frac{1}{k} - \frac{l_e}{\Omega_e} \right) (\dot{\boldsymbol{\beta}}_e \otimes \mathbf{n})^{\mathrm{S}} \right] \tag{63}$$

Now, from Equation (60c) and the expansion of $\boldsymbol{\xi}^{\mathrm{h}}(\mathbf{x})$ in Equation (58c)

$$\begin{aligned}
\delta\Pi_{\sigma}(\dot{\boldsymbol{\sigma}}^{\mathrm{h}},\dot{\boldsymbol{\Sigma}};\boldsymbol{\xi}^{\mathrm{h}}) = 0 \Rightarrow & \sum_{e=1}^{e=n_{\mathrm{elem}}} \int_{\Omega_e} (\dot{\boldsymbol{\sigma}}_e - \dot{\boldsymbol{\Sigma}}) : \boldsymbol{\xi}^{\mathrm{h}} \,\mathrm{d}\Omega \\
&= \sum_{e=1}^{e=n_{\mathrm{elem}}} \int_{\Omega_e} (\dot{\boldsymbol{\sigma}}_e - \dot{\boldsymbol{\Sigma}}) : \left(\bar{\boldsymbol{\xi}}_e + \mu_{\mathscr{S}}^{(e)} \frac{1}{k} (\boldsymbol{\alpha}_e \otimes \mathbf{n})^{\mathrm{S}} \right) \mathrm{d}\Omega \qquad (64) \\
&= \sum_{e=1}^{e=n_{\mathrm{elem}}} \left(\left[\Omega_e \dot{\boldsymbol{\sigma}}_e - \int_{\Omega_e} \dot{\boldsymbol{\Sigma}} \,\mathrm{d}\Omega \right] : \bar{\boldsymbol{\xi}}_e + \left[l_e \dot{\boldsymbol{\sigma}}_e \cdot \mathbf{n} - \int_{\mathscr{S}_e} \dot{\boldsymbol{\Sigma}} \cdot \mathbf{n} \,\mathrm{d}\mathscr{S} \right] \cdot \boldsymbol{\alpha}_e \right) \\
&= 0 \;\; \forall \bar{\boldsymbol{\xi}}_e \;\; \forall \boldsymbol{\alpha}_e \\
\Rightarrow & \left. \begin{array}{l} \left[\Omega_e \dot{\boldsymbol{\sigma}}_e - \displaystyle\int_{\Omega_e} \dot{\boldsymbol{\Sigma}} \,\mathrm{d}\Omega \right] = 0 \\ \left[l_e \dot{\boldsymbol{\sigma}}_e \cdot \mathbf{n} - \displaystyle\int_{\mathscr{S}_e} \dot{\boldsymbol{\Sigma}} \,\mathrm{d}\mathscr{S} \cdot \mathbf{n} \right] \end{array} \right\} \quad e \in \{1 \ldots n_{\mathrm{elem}}\} \qquad (65)
\end{aligned}$$

and solving for $\dot{\boldsymbol{\sigma}}_e$ in Equation (65), we get

$$\dot{\boldsymbol{\sigma}}_e = \frac{1}{\Omega_e} \int_{\Omega_e} \dot{\boldsymbol{\Sigma}} \,\mathrm{d}\Omega = \overline{\dot{\boldsymbol{\Sigma}}_{\Omega_e}} \qquad (66a)$$

$$\dot{\boldsymbol{\sigma}}_e \cdot \mathbf{n} = \frac{1}{l_e} \int_{\mathscr{S}_e} \dot{\boldsymbol{\Sigma}} \,\mathrm{d}\mathscr{S} \cdot \mathbf{n} = \overline{\dot{\boldsymbol{\Sigma}}_{\mathscr{S}}} \cdot \mathbf{n} \qquad (66b)$$

where $\overline{\dot{\boldsymbol{\Sigma}}_{\Omega_e}} = \frac{1}{\Omega_e} \int_{\Omega_e} \dot{\boldsymbol{\Sigma}} \,\mathrm{d}\Omega$ and $\overline{\dot{\boldsymbol{\Sigma}}_{\mathscr{S}}} = \frac{1}{l_e} \int_{\mathscr{S}_e} \dot{\boldsymbol{\Sigma}} \,\mathrm{d}\mathscr{S}$ are, respectively, the mean values of $\dot{\boldsymbol{\Sigma}}(\boldsymbol{\varepsilon}(\mathbf{x}))$ in Ω_e and $\mathscr{S}_e$. From Equation (66) it trivially follows

$$\overline{\dot{\boldsymbol{\Sigma}}_{\Omega_e}} \cdot \mathbf{n} = \overline{\dot{\boldsymbol{\Sigma}}_{\mathscr{S}}} \cdot \mathbf{n} \qquad (67)$$

which states the inner traction continuity condition (4e) in terms of the mean values of $\dot{\boldsymbol{\Sigma}}$. Equation (66b) can be rewritten in a more convenient format:

$$\frac{1}{l_e} \int_{\mathscr{S}_e} \dot{\boldsymbol{\Sigma}} \,\mathrm{d}\mathscr{S} \cdot \mathbf{n} - \frac{1}{\Omega_e} \int_{\Omega_e} \dot{\boldsymbol{\Sigma}} \,\mathrm{d}\Omega \cdot \mathbf{n} = \int_{\Omega_e} \left(\mu_{\mathscr{S}}^{(e)} \frac{1}{k} - \frac{l_e}{\Omega_e} \right) \dot{\boldsymbol{\Sigma}} \cdot \mathbf{n} \,\mathrm{d}\Omega = \mathbf{0} \qquad (68)$$

In summary, from Equations (64) and (68)

$$\delta\Pi_{\sigma}(\dot{\boldsymbol{\sigma}}^{\mathrm{h}},\dot{\boldsymbol{\Sigma}};\boldsymbol{\xi}^{\mathrm{h}}) = 0 \;\rightarrow \int_{\Omega_e} \left(\mu_{\mathscr{S}}^{(e)} \frac{1}{k} - \frac{l_e}{\Omega_e} \right) \dot{\boldsymbol{\Sigma}} \cdot \mathbf{n} \,\mathrm{d}\Omega = \mathbf{0} \quad \forall e \in \{1 \ldots n_{\mathrm{elem}}\} \qquad (69)$$

Finally, standard algebraic operations on Equation (60a), taking into account Equations (66) lead to

$$\delta\Pi_{u}(\dot{\boldsymbol{\sigma}}^{\mathrm{h}};\boldsymbol{\eta}^{\mathrm{h}}) = 0 \rightarrow \bigcup_{e=1}^{e=n_{\mathrm{elem}}} \int_{\Omega_e} \dot{\boldsymbol{\sigma}}_e : \nabla^{\mathrm{S}} \boldsymbol{\eta}^{\mathrm{h}} \,\mathrm{d}\Omega - G_{\mathrm{ext}}$$

$$= \bigcup_{e=1}^{e=n_{\text{elem}}} \int_{\Omega_e} \overline{\dot{\boldsymbol{\Sigma}}_{\Omega_e}} : \nabla^{\text{S}} \boldsymbol{\eta}^{\text{h}} \, \text{d}\Omega - G_{\text{ext}}$$

$$= \bigcup_{e=1}^{e=n_{\text{elem}}} \overline{\dot{\boldsymbol{\Sigma}}_{\Omega_e}} : \underbrace{\int_{\Omega_e} \nabla^{\text{S}} \boldsymbol{\eta}^{\text{h}} \, \text{d}\Omega}_{=\Omega_g \overline{\nabla^{\text{S}} \boldsymbol{\eta}}^{(e)}} - G_{\text{ext}}$$

$$= \bigcup_{e=1}^{e=n_{\text{elem}}} \underbrace{\Omega_e \overline{\dot{\boldsymbol{\Sigma}}_{\Omega_e}}}_{\int_{\Omega_e} \dot{\boldsymbol{\Sigma}} \, \text{d}\Omega} : \overline{\nabla^{\text{S}} \boldsymbol{\eta}}^{(e)} - G_{\text{ext}} = 0 \tag{70}$$

$$\Rightarrow \bigcup_{e=1}^{e=n_{\text{elem}}} \int_{\Omega_e} \overline{\nabla^{\text{S}} \boldsymbol{\eta}^{\text{h}}} : \dot{\boldsymbol{\Sigma}}(\boldsymbol{\varepsilon}^{\text{h}}) \, \text{d}\Omega - G_{\text{ext}} = 0 \quad \forall \boldsymbol{\eta}^{\text{h}} \in \mathscr{V}_{\mathbf{u}}^{0} \tag{71}$$

Remark 6

Notice from Equation (63) that the mixed approach recovers the same enhanced strain counterpart $\dot{\tilde{\boldsymbol{\varepsilon}}} = (\mu_{\mathscr{S}}^{(e)} \frac{1}{k} - \frac{l_e}{\Omega_e})(\dot{\boldsymbol{\beta}}_e \otimes \mathbf{n})^{\text{S}}$ postulated in Equation (37) for the assumed enhanced strain approach. However, in the mixed approach the term $\overline{\nabla^{\text{S}} \dot{\mathbf{u}}}^{(e)}$ in Equation (63) is constant and, therefore, so is the component $\nabla^{\text{S}} \dot{\mathbf{u}}^{(e)} \approx \overline{\nabla^{\text{S}} \dot{\mathbf{u}}}^{(e)}$ in Equation (51). This fact is expected to facilitate the cancellation of the elemental bulk strain $\dot{\boldsymbol{\varepsilon}}_{\Omega \setminus \mathscr{S}}^{(e)} = \nabla^{\text{S}} \dot{\mathbf{u}}^{(e)} - \frac{l_e}{\Omega_e} (\dot{\boldsymbol{\beta}}_e \otimes \mathbf{n})^{\text{S}}$ and contribute to alleviating the stress-locking phenomenon.

5.2.1. 2D implementation. Again, for the two-dimensional case and the four-noded quadrilateral element, the *B-format* formulation of the finite element method, from Equations (63), (69) and (71) reads

$$\left.\begin{aligned} \delta \Pi_u(\dot{\boldsymbol{\Sigma}}; \boldsymbol{\eta}^{\text{h}}) = 0 \\ \delta \Pi_\sigma(\dot{\boldsymbol{\sigma}}^{\text{h}}, \dot{\boldsymbol{\Sigma}}; \boldsymbol{\xi}^{\text{h}}) = 0 \end{aligned}\right\} \Rightarrow \bigcup_{e=1}^{e=n_{\text{elem}}} \left[\int_{\Omega_e} \bar{\mathbf{B}}^{(e)^{\text{T}}} \cdot \{\dot{\boldsymbol{\Sigma}}\} \, \text{d}\Omega - \dot{\mathbf{F}}^{\text{ext}(e)} \right] = \mathbf{0} \tag{72}$$

$$\{\dot{\boldsymbol{\varepsilon}}\}^{(e)} = \bar{\mathbf{B}}^{(e)} \cdot \dot{\mathbf{d}}^{(e)}$$

$$\dot{\mathbf{d}}^{(e)} = [\dot{\mathbf{d}}_1, \ \dot{\mathbf{d}}_2, \ \dot{\mathbf{d}}_3, \ \dot{\mathbf{d}}_4, \ \dot{\boldsymbol{\beta}}_e]^{\text{T}} \tag{73}$$

$$\bar{\mathbf{B}}^{(e)} = [\bar{\mathbf{B}}_1^{(e)}, \ \bar{\mathbf{B}}_2^{(e)}, \ \bar{\mathbf{B}}_3^{(e)}, \ \bar{\mathbf{B}}_4^{(e)}, \ \mathbf{G}^{(e)}]$$

$$\bar{\mathbf{B}}_i^{(e)} = \begin{bmatrix} \overline{\partial_x N_i^{(e)}} & 0 \\ 0 & \overline{\partial_y N_i^{(e)}} \\ \overline{\partial_y N_i^{(e)}} & \overline{\partial_x N_i^{(e)}} \end{bmatrix}; \quad \bar{(\cdot)}^{(e)} \stackrel{\text{def}}{=} \underbrace{\frac{1}{\Omega_e} \int_{\Omega_e} (\cdot) \, \text{d}\Omega}_{\text{mean value of } (\cdot) \text{ on } \Omega_e} \tag{74}$$

$$\mathbf{G}^{(e)} = \left(\mu_{\mathscr{S}}^{(e)} \frac{1}{k} - \frac{l_e}{\Omega_e} \right) \begin{bmatrix} n_x & 0 \\ 0 & n_y \\ n_y & n_x \end{bmatrix}$$

Remark 7

For practical purposes the computation of the mean elemental values $(\bar{\cdot})^{(e)}$ referred to in Equation (74) can be approximately (or even exactly, for undistorted elements) computed, for the quadrilateral element, through sampling at the centre of the element. Consequently, by comparison of Equations (47) and (74) the mixed M4n element can be retrieved from the symmetric S4n element by reducing the four regular sampling points (PG1–PG4 in Figure 2(e)) to one placed at the centre of the element (RSP in that figure). Therefore, the classical link between mixed elements and reduced integration [26] is also recovered for finite elements with embedded discontinuities.

6. STRAIN RE-ENHANCEMENT: ELEMENT E4n

Next strategy is based on providing new terms to the enhanced strain component ($\dot{\tilde{\boldsymbol{\varepsilon}}}$ in Equation (28)) of the symmetric element S4n. Two conditions are required on this enhancement:

(i) Fulfil the orthogonality condition (27):

$$\int_{\Omega} \dot{\tilde{\boldsymbol{\varepsilon}}} : \boldsymbol{\tau} \, \mathrm{d}\Omega = 0 \quad \forall \dot{\tilde{\boldsymbol{\varepsilon}}} \in \mathscr{V}_{\tilde{\boldsymbol{\varepsilon}}} \; \forall \boldsymbol{\tau} \in \mathscr{V}_{\boldsymbol{\sigma}} \tag{75}$$

(ii) Include linear polynomial terms to contribute to alleviate the stress-locking phenomenon.

With these conditions in mind, the following strain enhancement is proposed:

$$\dot{\tilde{\boldsymbol{\varepsilon}}}^{\mathrm{h}(e)} = \underbrace{\left(\mu_{\mathscr{S}}^{(e)} \frac{1}{k} - \frac{l_e}{\Omega_e}\right) (\dot{\boldsymbol{\beta}}_e \otimes \mathbf{n})^{\mathrm{S}}}_{\dot{\tilde{\boldsymbol{\varepsilon}}}_1^{(e)}} + \underbrace{\frac{1}{J} s \dot{\mathbf{S}}_e + \frac{1}{J} t \dot{\mathbf{T}}_e}_{\dot{\tilde{\boldsymbol{\varepsilon}}}_2^{(e)}} \tag{76}$$

where s and t stand for the isoparametric coordinates of the standard four-noded quadrilateral and J is the jacobian of the isoparametric transformation relating differential areas in the regular and isoparametric spaces through

$$\mathrm{d}\Omega = J \, \mathrm{d}s \, \mathrm{d}t \tag{77}$$

In Equation (76) $\dot{\tilde{\boldsymbol{\varepsilon}}}_1^{(e)}$ is the basic strain enhancement, already present in the basic S4n element, and $\dot{\tilde{\boldsymbol{\varepsilon}}}_2^{(e)}$ is a *re-enhancement* of the strain field that supplies the required linear polynomial components to the elemental bulk strain. The values $\{\dot{\mathbf{S}}_e\} = [\dot{S}_{xx}, \dot{S}_{yy}, \dot{S}_{xy}]_e^{\mathrm{T}}$ and $\{\dot{\mathbf{T}}_e\} = [\dot{T}_{xx}, \dot{T}_{yy}, \dot{T}_{xy}]_e^{\mathrm{T}}$ are (constant) intensity factors that constitute six (for the 2D problem) additional degrees of freedom of the element. From expression (76) it is clear that the orthogonality condition (75) is fulfilled for the elementwise constant assumed stress field

in Equation (35) since

$$\int_{\Omega_e} \dot{\tilde{\boldsymbol{\varepsilon}}}_1^{(e)} : \boldsymbol{\tau}_e \, \mathrm{d}\Omega = \int_{\Omega_e} \left(\mu_{\mathscr{S}}^{(e)} \frac{1}{k} - \frac{l_e}{\Omega_e} \right) (\dot{\boldsymbol{\beta}}_e \otimes \mathbf{n})^{\mathrm{S}} : \boldsymbol{\tau}_e \, \mathrm{d}\Omega$$

$$= \underbrace{\int_{\Omega_e} \left(\mu_{\mathscr{S}}^{(e)} \frac{1}{k} - \frac{l_e}{\Omega_e} \right) \mathrm{d}\Omega}_{l_e - l_e = 0} (\dot{\boldsymbol{\beta}}_e \otimes \mathbf{n})^{\mathrm{S}} : \boldsymbol{\tau}_e = 0 \tag{78}$$

$$\int_{\Omega_e} \dot{\tilde{\boldsymbol{\varepsilon}}}_2^{(e)} : \boldsymbol{\tau}_e \, \mathrm{d}\Omega = \int_{\Omega_e} \frac{1}{J} (s \dot{\mathbf{S}}_e + t \dot{\mathbf{T}}_e) : \boldsymbol{\tau}_e \, \mathrm{d}\Omega$$

$$= \underbrace{\int_{-1}^{+1} \int_{-1}^{+1} s \, \mathrm{d}s \, \mathrm{d}t}_{=0} \dot{\mathbf{S}}_e : \boldsymbol{\tau}_e + \underbrace{\int_{-1}^{+1} \int_{-1}^{+1} t \, \mathrm{d}s \, \mathrm{d}t}_{=0} \dot{\mathbf{T}}_e : \boldsymbol{\tau}_e = 0 \tag{79}$$

6.1. 2D implementation

In view of the preceding formulation, the 2D implementation of element E4n becomes similar to that of the element S4n in Equations (45) and (47) but including the additional enhanced strain terms in Equation (76). That is

$$\left.\begin{array}{r} \delta\Pi_u(\dot{\boldsymbol{\Sigma}}; \boldsymbol{\eta}^{\mathrm{h}}) = 0 \\ \delta\Pi_\sigma(\dot{\boldsymbol{\sigma}}^{\mathrm{h}}, \dot{\boldsymbol{\Sigma}}; \boldsymbol{\xi}^{\mathrm{h}}) = 0 \end{array}\right\} \Rightarrow \bigcup_{e=1}^{e=n_{\mathrm{elem}}} \left[\int_{\Omega_e} \mathbf{B}^{(e)^{\mathrm{T}}} \cdot \{\dot{\Sigma}\} \, \mathrm{d}\Omega - \dot{\mathbf{F}}^{\mathrm{ext}(e)} \right] = \mathbf{0} \tag{80}$$

$$\begin{aligned} \{\dot{\boldsymbol{\varepsilon}}\}^{(e)} &= \mathbf{B}^{(e)} \cdot \dot{\mathbf{d}}^{(e)} \\ \dot{\mathbf{d}}^{(e)} &= [\dot{\mathbf{d}}_1, \ \dot{\mathbf{d}}_2, \ \dot{\mathbf{d}}_3, \ \dot{\mathbf{d}}_4, \ [\dot{\boldsymbol{\beta}}_e, \{\dot{\mathbf{S}}_e\}, \{\dot{\mathbf{T}}_e\}]]^{\mathrm{T}} \\ \mathbf{B}^{(e)} &= [\mathbf{B}_1^{(e)}, \ \mathbf{B}_2^{(e)}, \ \mathbf{B}_3^{(e)}, \ \mathbf{B}_4^{(e)}, \ \mathbf{G}^{(e)}] \\ \mathbf{B}_i^{(e)} &= \begin{bmatrix} \partial_x N_i^{(e)} & 0 \\ 0 & \partial_y N_i^{(e)} \\ \partial_y N_i^{(e)} & \partial_x N_i^{(e)} \end{bmatrix} \end{aligned} \tag{81}$$

$$\mathbf{G}^{(e)} = \underbrace{\begin{bmatrix} \gamma n_x & 0 \\ 0 & \gamma n_y \\ \gamma n_y & \gamma n_x \end{bmatrix}}_{\dot{\tilde{\boldsymbol{\varepsilon}}}_1} \underbrace{\begin{bmatrix} s & 0 & 0 & t & 0 & 0 \\ 0 & s & 0 & 0 & t & 0 \\ 0 & 0 & s & 0 & 0 & t \end{bmatrix}}_{\dot{\tilde{\boldsymbol{\varepsilon}}}_2} \tag{82}$$

$$\gamma = \left(\mu_{\mathscr{S}}^{(e)} \frac{1}{k} - \frac{l_e}{\Omega_e} \right)$$

where the eight internal degrees of freedom $[\dot{\boldsymbol{\beta}}_e, \{\dot{\mathbf{S}}_e\}, \{\dot{\mathbf{T}}_e\}]$ can be condensed at elemental level.

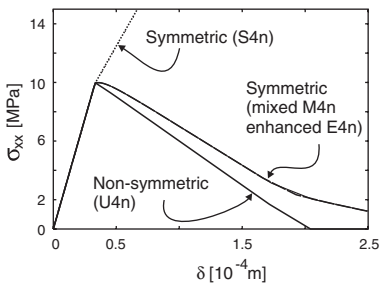

Figure 4. Homogeneous plate: stress σ_{xx} vs displacement δ curves for different elements.

7. NUMERICAL TESTS

7.1. Homogeneous plate

The basic test of Section 4 and Figure 3 is now repeated using the modified elements M4n and E4n. The results, again in terms of σ_{xx}–δ curves, are presented in Figure 4 together with the ones obtained with the original element S4n and the exact result (U4n).

It can be observed the dramatic reduction in the stress-locking effect obtained with the new elements which prove the effectiveness of the adopted strategies. Besides, one can observe that the results obtained with element M4n (mixed strategy) and element E4n (re-enhancement strategy) are very similar to each other, which shows that the improvement reasoning based on the *cancellation* of the bulk strain, stated in Section 4 and implemented in two different strategies, was essentially correct.

7.2. Notched specimen

In order to assess the performance of the proposed strategies in more complex problems, the test of Figure 5(a) is also considered. It is a notched specimen whose experimental testing is reported in Reference [27]. The couples of forces F_1 and F_2 are progressively applied, as it is indicated, in Figure 5(b) in order to induce a mixed mode crack which develops from the notch tip with an inclination angle of 71° (see Figure 5(c)). For the numerical simulation the same material model (isotropic continuum damage with linear softening) as in the previous case has been adopted, with the following parameters: the elastic modulus and Poisson's ratio are $E = 30580$ Mpa and $v = 0.2$ respectively, the fracture energy $G_f = 100$N/m and the tensile strength is assumed to be $\sigma_u = 3$MPa. The width of the specimen is $t = 50.8$ mm.

The results, in terms of the applied force versus the CMOD, obtained with the U4n element, the original S4n element and the modified symmetric M4n and E4n elements, as well as the experimental values from the above reference, are presented in Figure 5(d). Again the dramatic improvement, in terms of the numerical stress-locking effect, obtained with the devised strategies in comparison with the original symmetric element S4n can be observed. Also the iso-displacement curves shown in Figure 5(e) display a modelled discontinuity that matches very well the experimental crack.

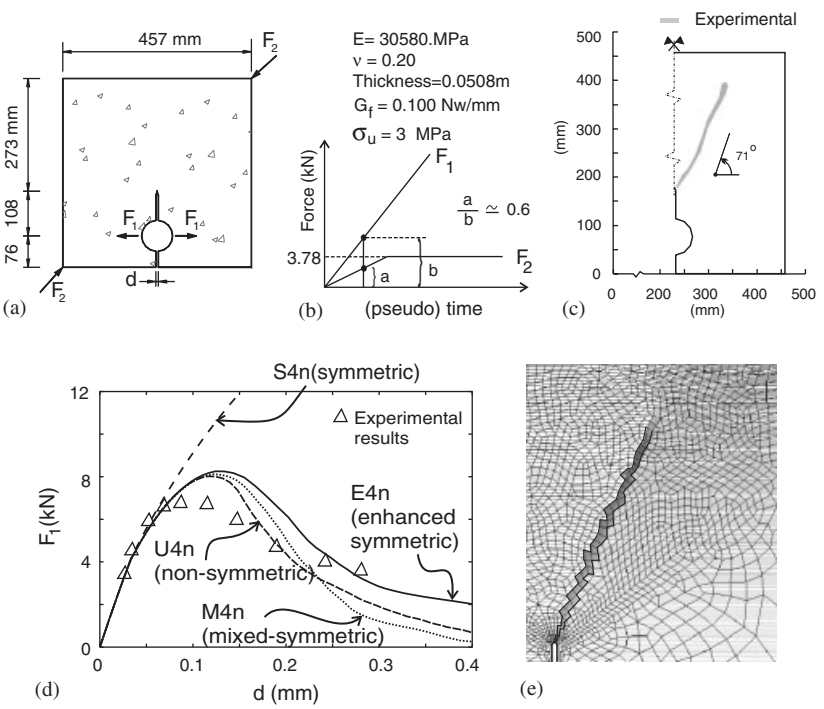

Figure 5. Notched specimen: (a) geometrical model; (b) imposed external loading along time; (c) observed crack in the experimental test; (d) load F_1 vs opening displacement d for different finite elements; and (e) displacement contours ($d = 0.04$ mm).

7.3. Three point notched beam

We consider now the three point notched concrete beam, in plane strain, shown in Figure 6(a). Experimental data for this test have been presented by Peterson [28].

The concrete post-critical behaviour is modelled by the same isotropic continuum damage model than in Reference [15]. The material parameters are taken: $E = 30580$ Mpa, $v = 0.2$ and the fracture energy $G_f = 126$ N/m. The tensile strength is taken $\sigma_u = 3.4$ MPa. The width of the specimen is $t = 100$ mm. The mesh consists of 615 quadrilaterals refined near the notch tip.

A crack opening in mode I is expected to develop from the notch tip, propagating in the vertical direction through the beam, as shown in Figure 6(b). The plots in Figure 6(c) and (d) correspond, respectively, to the load F vs the vertical displacement δ curves using linear and exponential softening laws.

Once again the striking behaviour already observed in the previous simulations can be noticed: the M4n and E4n elements dramatically reduce the stress-locking phenomenon exhibited by the original S4n element, and provide a response that is very close to the one obtained with the non-symmetric (U4n) element.

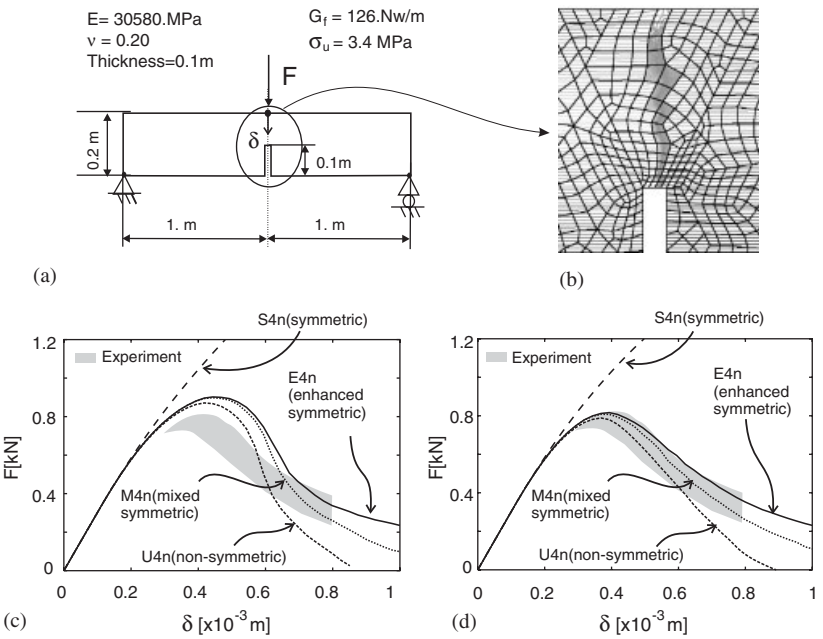

Figure 6. Three points notched beam: (a) geometrical model; (b) discontinuity path; (c) results for linear softening; and (d) results for exponential softening.

8. CONCLUDING REMARKS

Throughout this work we have explored the possibility of using statically consistent symmetric elements with embedded discontinuities to capture strong discontinuities. As a matter of fact it has been shown that the use of mixed (M4n element) or assumed enhanced strain (E4n element) techniques contribute to substantially alleviate the strain-locking phenomenon appearing in the original S4n element.

In essence these techniques are intended for recovering the capacity of the non-symmetric element U4n to reproduce rigid body motions of the portions of the elements split up into by the discontinuity, while keeping the symmetric character and variational consistency of the original symmetric S4n element.

An important issue, that has not been addressed so far, is the stability properties of the derived elements. It is well-known in the literature that the use of mixed element techniques [28] and assumed enhanced strain techniques [24] may introduce spurious singular modes whose propagation through the finite element mesh can destroy both the reliability of the solution and the convergence of the non-linear problem. For instance: it is known that the four-noded element with reduced integration (one sampling point) considered here in element M4n, leads to the development and propagation of the so called hour-glass spurious modes [22]. Also the linear re-enhancement modes, $\dot{\tilde{\boldsymbol{\varepsilon}}}_2^{(e)}$ in Equation (76), considered for the E4n element do not fulfil the stability condition ($\mathscr{V}_{\tilde{\boldsymbol{\varepsilon}}} \cap \mathscr{V}_{\boldsymbol{\varepsilon}} = \{0\}$) [24].

However, there is a crucial aspect in the way that the elements derived in this work are implemented and that makes their stability behaviour very different from the classical ones.

Throughout this work, those finite element formulations have been derived and presented for the BVP in rate (incremental) form (see Equations (4), (45), (72) or (80)). This allows to consider the problem as a sequence, along time, of incremental problems, each one having its own finite element formulation. As a matter of fact the implementation is done in such a way that the *modifications on the basic element S4n* that lead to the derived elements M4n and E4n, *are effective only for the band of elements that captures the discontinuity and only beyond the time that this discontinuity appears*. The elements outside this band behave as the original S4n since they do not exhibit the stress-locking problem that the modified elements try to overcome. This decreases the number of elements affected by the reduced integration or re-enhancement techniques to a single band of essentially one element bandwidth. Consequently *the development and propagation of spurious instability modes are extremely restrained*. In addition, the computational costs associated to the presence of new degrees of freedom (for the re-enhancement strategy) are then very small.

Although specific stability analyses have not been conducted in this paper, and they are left for subsequent works, during the numerical simulations presented above, and others carried out during this study, the possible instability modes have not been observed and have not placed special difficulties on the numerical procedure. However, the authors are aware that this cannot be generalized to any type and size of the problems, and that specific studies on the stability issue should be carried out in the future.

Also the possibility of using some of the developed elements to dispense with the discontinuity tracking algorithm should be explored in subsequent works.

ACKNOWLEDGEMENTS

This work has been done with the support of the Spanish Ministry of Science and Technology under grants MAT-2001-3863-C03-03 and MAT-2000-0436. This support is gratefully acknowledged.

REFERENCES

1. Dvorkin EN, Cuitino AM, Gioia G. Finite elements with displacement embedded localization lines insensitive to mesh size and distortions. *International Journal for Numerical Methods in Engineering* 1990; **30**:541–564.
2. Larsson R, Runesson K, Ottosen NS. Discontinuous displacement approximation for capturing plastic localization. *International Journal for Numerical Methods in Engineering* 1993; **36**:2087–2105.
3. Lofti HR, Benson Shing P. Embedded representation of fracture in concrete with mixed finite elements. *International Journal for Numerical Methods in Engineering* 1995; **38**:1307–1325.
4. Simo J, Oliver J. A new approach to the analysis and simulation of strong discontinuities. In *Fracture and Damage in Quasi-brittle Structures*, Bazant ZP *et al.* (eds). E & FN. Spon, 1994; 25–39.
5. Oliver J, Simo J. Modelling strong discontinuities by means of strain softening constitutive equations. In *Proceedings of the EURO-C 1994 Computer Modeling of concrete structures*, Mang H *et al.* (eds). Pineridge Press: Swansea, 1994; 363–372.
6. Oliver J. Modeling strong discontinuities in solid mechanics via strain softening constitutive equations. Part 2: Numerical simulation. *International Journal for Numerical Methods in Engineering* 1996; **39**(21):3601–3623.
7. Armero F, Garikipati K. An analysis of strong discontinuities in multiplicative finite strain plasticity and their relation with the numerical simulation of strain localization in solids. *International Journal of Solids and Structures* 1996; **33**(20–22):2863–2885.
8. Larsson R, Runesson K, Sture S. Embedded localization band in undrained soil based on regularized strong discontinuity theory and finite element analysis. *International Journal of Solids and Structures* 1996; **33**(20–22):3081–3101.
9. Celigoj CC. On strong discontinuities in an elastic solids. A finite element approach taking a frame indifferent gradient of the discontinuous displacements. *International Journal for Numerical Methods in Engineering* 2000; **49**:769–796.

10. Belytschko T, Moes N, Usui S, Parimi C. Arbitrary discontinuities in finite elements. *International Journal for Numerical Methods in Engineering* 2001; **50**:993–1013.
11. Wells GN, Sluys LJ. A new method for modelling cohesive cracks using finite elements. *International Journal for Numerical Methods in Engineering* 2001; **50**:2667–2682.
12. Regueiro RA, Borja RI. Plane strain finite element analysis of pressure sensitive plasticity with strong discontinuity. *International Journal of Solids and Structures* 2001; **38**:3647–3672.
13. de Borst R, Sluys LJ, Muhlhaus HB, Pamin J. Fundamental issues in finite element analyses of localization of deformation. *Engineering Computations* 1993; **10**:99–121.
14. Jirasek M. Comparative study on finite elements with embedded discontinuities. *Computer Methods in Applied Mechanics and Engineering* 2000; **188**:307–330.
15. Oliver J. Continuum modelling of strong discontinuities in solid mechanics. In *Computational Plasticity. Fundamentals and Applications*, vol. 1, Owen DRJ, Onate E (eds). Pineridge Press: Swansea, 1995; 455–479.
16. Oliver J, Cervera M, Manzoli O. On the use of J2 plasticity models for the simulation of 2D strong discontinuities in solids. In *Proceedings of the International Conference on Computational Plasticity*, Owen DRJ, Onate E, Hinton E (eds). C.I.M.N.E.: Barcelona (Spain), 1997; 38–55.
17. Oliver J, Cervera M, Manzoli O. On the use of strain-softening models for the simulation of strong discontinuities in solids. In *Material Instabilities in Solids*, de Borst R, van der Giessen E (eds), chapter 8. Wiley: New York, 1998; 107–123.
18. Oliver J. The strong discontinuity approach: an overview. In *Computational Mechanics. New Trends and Applications.* (*WCCM98*) *Proceedings* (*CD-ROM*) *of the IV World Congress on Computational Mechanics*, Idelsohn S, Oate E, Dvorkin EN (eds). CIMINE: Barcelona, 1998.
19. Oliver J, Cervera M, Manzoli O. Strong discontinuities and continuum plasticity models: The strong discontinuity approach. *International Journal of Plasticity* 1999; **15**(3):319–351.
20. Oliver J, Huespe A, Pulido MDG, Chaves E. From continuum mechanics to fracture mechanics: the strong discontinuity approach. *Engineering Fracture Mechanics* 2002; **69**(2):113–136.
21. Oliver J, Huespe AE, Pulido MDG, Samaniego E. On the strong discontinuity approach in finite deformation settings. *International Journal for Numerical Methods in Engineering*, submitted.
22. Zienkiewicz OC, Taylor RL. *The Finite Element Method.* Butterworth-Heinemann: Oxford, UK, 2000.
23. Simo JC, Hughes TJR. *Computational Inelasticity*. Springer: Berlin, 1998.
24. Simo JC, Rifai S. A class of mixed assumed strain methods and the method of incompatible modes. *International Journal for Numerical Methods in Engineering* 1990; **29**:1595–1638.
25. Oliver J. On the discrete constitutive models induced by strong discontinuity kinematics and continuum constitutive equations. *International Journal of Solids and Structures* 2000; **37**:7207–7229.
26. Malkus DS, Hughes TJR. Mixed finite element methods—reduced and selective integration techniques: a unification of concepts. *Computer Methods in Applied Mechanics and Engineering* 1978; **15**:63–81.
27. Kobayashi AS, Hawkins MN, Barker DB, Liaw BM. Fracture process zone of concrete. In *Application of Fracture Mechanics to Cementitious Composites*, Shah SP (ed.). Marinus Nujhoff Publ.: Dordrecht, 1985; 25–50.
28. Peterson PE. Crack Growth and development of fracture zones in plain concrete and similar materials. Technical Report, Division of building material, 1981. Report No. 1006.

